INVESTIGATION OF ELECTRONIC CORRELATIONS

IN NANOSTRUCTURES

DISSERTATION

zur Erlangung des akademischen Grades
doctor rerum naturalium (Dr. rer. nat.)

vorgelegt der
Matematisch-Naturwissenschaftlich-Technischen Fakultät
(matematisch-naturwissenschaftlich Bereich)
der Martin-Luther-Universität Halle-Wittenberg

von Herrn **Oleg Kidun**

geb. am 25.02.1969 in Maxatikha, Russland

Gutachterin/Gutachter:

1. Prof. P. Bruno
2. Prof. W. Hergert
3. Prof. N. Kabachnik

Halle/Saale, Oktober 2002

verteidigt am 09.04.2003

Die Liste der Veröffentlichungen:

1. O. Kidun, N. Fominykh, J. Berakdar, Scattering and bound-state problems with nonlocal potentials: application of the variable phase approach, J. Phys. A, 35, p. 9413, 2002

2. N. Fominykh, O. Kidun, A. Ernst, J. Berakdar, Ejection of a correlated electron pair from a quantum dot, submitted to J. Phys. B.

3. O. Kidun, J. Berakdar, Manifestation of charge-density fluctuations in metal clusters: suppression of the ionization channel, Phys. Rev. Lett., 87, no.26, p. 263401, 2001

4. O. Kidun, J. Berakdar, Excitation spectra of free fullerene clusters, Surface Science, 507-510, p. 662, 2002

5. O. Kidun, J. Berakdar, Correlation effects in the (e,2e) process on C_{60}, Phys. Solid State, 44(3), p. 567, 2002

6. O. Kidun, J. Berakdar, Nonlocal variable phase method applied to ionization of C_{60} by electron impact, in the book "Many-particle spectroscopy of Atoms, Molecules, Clusters and Surfaces", Plenum, NY, p. 395, 2001

7. J. Berakdar, O. Kidun, A. Ernst, Manifestations of electronic correlation in finite and extended systems, in the book "(e,2e) and Polarization Phenomena", p. 64, 2001

Table of Contents

Acknowledgements

I would like to thank Jamal Berakdar, my supervisor, for his many suggestions and constant attention and support during this research. Professor Patrick Bruno expressed his interest in my work and I appreciate our discussions with him. I had the pleasure of short but impressive conversation with Manfred Taut, and long but also impressive discussions with Vitalii Dugaev.

I am also thankful to Professor I. V. Abarenkov for his involuntary guidance through the early years of chaos and confusion. Professor A. S. Shulakov, Professor A. S. Vinogradov and Professor A. P. Pavlychev provided me with friendly encouragement during my graduate studies in Russia.

Finally, I wish to thank Natasha Fominykh for her existance.

O. Kidun
Halle, Germany
November 5, 2002

Chapter 1

Introduction

Research of clusters and other nanoparticles has generated a new rapidly developing interdisciplinary branch, in which knowledge and methodologies from atomic, molecular and solid state physics have been extensively combined. Alkali metal clusters were the first systems for which the electronic shell structure was observed. Many properties of these clusters can be explained by delocalized valence electrons. On the other hand, noble gases form structures with icosahedral symmetry, also typical for the clusters of fullerene family. In all these systems the account of inter-electron interaction can modify or drastically change the simple independent-electron theory results. The catch-all phrase 'electron correlation effects' is often used to describe the resulting new phenomena.

During the last decade scattering experiments based on the coincidence techniques have emerged as a powerful tool for getting valuable and sometimes even unique information about electron dynamics in atoms, molecules and solids. Theoretical support of such correlation-accented experiments represents a real challenge for the scientific community, because it has to deal with the solution of the many-body problems for

the systems with a large number of electrons, but not too large to make solid-state approximations possible. Therefore the development of new analytical methods and numerical techniques becomes vital.

Hartree-Fock approximation provides the necessary background for the treatment of correlations in the perturbative theories. Its main feature is that it is based on the solution of the nonlocal potential problem, representing severe numerical difficulties. The first part of our work is devoted to the development of the new framework specially suited for this purpose. We extend the Variable Phase Approach [7, 21] onto the nonlocal potential problems. Namely, we derive the equation for the scattering amplitude function, which allows to solve both the eigenvalue and the scattering problems. Then we reformulate the Hartree-Fock problem in terms of this approach. Next, we propose the efficient finite-difference scheme for its numerical solution, providing the calculation efforts which are of the same order as those for the local potential case.

Having prepared this analytical and practical support, we are able to go beyond the mean-field concept and to apply the Random Phase with Exchange Approximation for the rigorous treatment of screening in clusters, which is crucial for the evaluation of dynamic properties in terms of collective excitations. We consider the electron-impact ionization of C_{60} and metal clusters and show that the account of the dynamic polarizability of clusters allows to explain certain features of (e,2e) spectra, hitherto not reproduced in the calculations. The effect of exchange interaction is considered by the positron-impact ionization of clusters.

Next scattering reaction dominated by electron correlations is double or multiple photoionization, in which a single photon with sufficient energy ionizes two or more electrons simultaneously. In order to be involved in such reactions, electrons of the

target have to be strongly correlated. We use the Statistical Energy Deposition Model for the calculation of the different multiple photoionization cross sections of fullerene. It allows to estimate, in average, the strength of correlations through the comparison of the magnitudes of the single-, double- and n-fold photoionization cross sections.

The detailed knowledge on the multi-electron behavior of the system is most readily incorporated into the exact many-electron wave function. The narrow class of exactly solvable problems in few-body physics gives a unique opportunity to test approximate theories and to clarify the hidden features of the many-body processes. As an alternative to different approximate treatments of the previous chapters, at the end we derive the double photoionization matrix element for the systems, admitting the description by the parabolic confinement, using the exact two-electron wave function.

In Chapter 2 an overview of the electronic properties and the spectroscopic investigations of correlations in clusters and fullerenes is given.

Variable Phase Approach is extended to the solution of the nonlocal potential problems in Chapter 3, where we also derive the finite-difference scheme for their numerical solution.

Using these results, in Chapter 4 we reformulate the Hartree-Fock problem and provide an example of the calculations.

The essence and the equations of the Random Phase Approximation are discussed in Chapter 5.

4

Electronic correlation as revealed by the electron- and positron-impact ionization of fullerene and metal clusters is considered in Chapter 6 basing on the Random Phase calculations.

Chapter 7 deals with the single- and multiple photoionization of C_{60}. The diffraction of the photoelectron wave on the fullerene shell is shown to be a prominent feature of these processes.

The exact two-electron wave function and the double photoionization cross section of the quantum dot are calculated in Chapter 8. The mapping of the two-electron density onto the double photoionization spectra is suggested.

Chapter 9 summarizes the results of the dissertation.

Chapter 2

Clusters and fullerenes

2.1 Experiments and theories

In the past decades, an enormous progress in the miniaturization of electronic and mechanical devices caused an increasing amount of research dedicated to the physics of clusters. Among many important contributions of cluster science, one of the most significant is that a cluster in itself can serve as a unique test system for checking the validity of new theories developed for the mesoscopic physics.

The role of size effects has been a primary motivating factor in metal clusters research. It is based on the understanding that the shape of the clusters will be reflected in the electronic structure, especially at the spatial dimensions that are of the same order of magnitude as the Fermi wavelength. It was found out that metal clusters composed of a specific number of atoms are much more stable. Such clusters, called 'magic number clusters', are well described by the so-called shell model. In this model, the electron-nucleus many-body problem is reduced to that for a system of delocalized valence electrons, placed in the uniform positively-charged background. The density of the latter is a parameter that is usually chosen to be the bulk density or to reproduce the experimentally established ionization potentials of the clusters.

In doing this, all electrons are confined to a spherical potential well, as if the cluster were a single atom. Correspondingly, their electronic structure [25] consists of shells, where electrons on a given shell have the same radial and angular momentum quantum numbers. Each shell can contain $2(2\ell + 1)$ electrons. The clusters in which all shells are closed represent the magic number objects and are easily distinguishable via mass-spectrometry techniques (see e.g. [76]).

The optical response of alkali-metal clusters has been measured for a large variety of systems (see e.g. [16, 25, 26, 63, 79]). The energy dependence of the photoionization cross section of clusters with filled electronic shells is especially simple and shows a broad resonance around a frequency typical for the corresponding bulk metals. This has also lead to an interpretation in terms of the jellium model.

On the other hand, a typical example of magic number semiconductor clusters is fullerene (C_{60}, C_{70}, C_{74}, C_{80}, ...). It is not only the high symmetry and the unusual structure that makes these molecules extremely attractive objects to study. Fullerene family exhibits rich variety of physical and chemical properties [22, 35, 69], which are defined, to a large extent, by characteristics and interactions of the electrons in the valence electronic shells. Being good electron acceptors, fullerenes are capable of forming a great number of new compounds. Their shell-like structure provides enough space for introducing another atoms inside, thus changing the properties of the molecule.

As a many-electron system the single fullerene molecule demonstrates the collection of phenomena, arising due to the electronic correlations. Because of the unsaturated character of the C-C bonds on the fullerene, there are plenty of electronic states delocalized over the molecular surface and freely available not only for donors but also

for interaction with each other. Electron-electron and electron-hole interactions determine, for example, electric dipole polarizability [23], giant plasmon resonances [13, 39], anomalously strong screening upon collision with ions [61], non-linear dipole response and ionization upon femtosecond laser pulses [9], on-site Coulomb energy [18, 53], i.e. the energy cost of placing two electrons on the same fullerene molecule. This last quantity, characterizing a single molecule, is responsible for metallic or insulating behavior of the materials [35].

All known electron spectroscopies (for the review see e.g. [69]), such as direct and inverse photoemission spectroscopy [11, 68], X-ray absorption, resonant photoemission, Auger electron spectroscopy, electron energy loss spectroscopy and (e,2e) (or electron-momentum) spectroscopy, have been applied for studying cluster properties. All of them, and especially those from the new generation of experiments, based on coincidence techniques [88], stimulate the development of reliable theoretical models describing the phenomena under consideration.

The spherical jellium model is the starting point for electronic structure calculations. Theoretical approaches, developed in atomic, molecular and nuclear physics and now used in the cluster science, are as follows: the Hartree-Fock approximation for the calculation of the electronic states and structural optimization [44, 54]; different density functional approaches for the description of the ground-state properties [15, 78]; Monte-Carlo [60] and molecular dynamics [51] simulations of the thermodynamical and other physico-chemical properties; random phase approximation for the calculation of the dielectric response to external fields [24, 38], and the list continues.

2.2 Density functional and Hartree-Fock methods

The density functional theory (DFT), that originated from the pioneer work of Kohn and Hohenberg [40], proved to be very successful in describing the ground state of finite many-electron systems. DFT is based on the one-to-one correspondence between particle densities of the considered systems and external potentials acting upon these particles. In application to the calculations of the electronic structure of clusters [10, 30, 90], DFT is usually used in the local density approximation (LDA), i.e. it is assumed that the exchange and correlation terms should be treated locally and on equal footing, and thus cast into a local density-dependent potential. The construction of the ground state is then easily performed within an effective mean-field theory. For bulk metal, the LDA seems indeed to be more natural than the HF approximation, which fails to reproduce a finite density of states at the Fermi level. However, for finite systems, neither of two methods has proven its superiority. In spite of the significant differences in the theoretical justification of both theories, they provide rather close results, and a comparison of calculations is a matter of detailed investigations [55, 65, 66]. When choosing between the two theories, one should be aware of two systematic differences. First, due to the presence of the Fock exchange term, compensating for the interaction of an electron with itself, the HF theory provides the correct $1/r$ asymptotic behavior of the one-electron mean-field potential. This is extremely important for the calculation of the observables, sensitive to the long-range potential slope and to the outer parts of the electronic wave function. As for the LDA, it fails to provide the asymptotic fall-off of the mean-field potential, and the additional self-interaction corrections are required [62]. However, the latter represent an *adhoc* prescription and can not be improved or extended in terms of perturbation

theory. Second, in DFT only the existence of the unique exchange-correlation functional is established. A question on how one can construct it for any given system is left aside. Therefore, the results strongly depend on the availability of good approximations for the exchange-correlation functionals and their interpretation is not straightforward. In contrast, the HF approximation can serve as a background for a systematic development of many-body theories and allows one to construct models on the basis of fundamental physical principles, which can then be refined by extending the quality of the approximations. Due to the nonlocal nature of the Fock exchange term (see Appendix), the calculations become considerably more complicated and time consuming than in the LDA approach. Therefore the next chapter deals with the development of the new conceptual framework and the numerical algorithms for the calculation of the nonlocal potential problems. In chapter 4 we will apply these results to the solution of the HF problem.

Chapter 3

Variable phase approach and its application to the nonlocal potential problems

3.1 General overview

In the early sixties, an elegant approach was developed independently by Calogero [21] and Babikov [7], in which the solution of the quantum-mechanical problems was formulated in terms of observables (e.g. scattering phase shifts and scattering amplitudes), rather than by means of the wave functions. According to this, the approach was referred to as the variable phase approach (VPA), or phase-amplitude method. The VPA relies on the fact that any second order differential equation (DE), in particular, the Schrödinger equation, is equivalent to a pair of first-order DE's for the phase and the amplitude functions. In [21, 7] it is shown that one can separate one of these two equations so that it becomes independent of the second one. It may happen that the solution of only one of the two DE's is enough for the solution of the problem, e.g. it is sufficient to know only the scattering phase shifts in order to calculate the scattering cross section. The solution of the second DE allows to completely restore

the wave function and to get information equivalent to the traditional solution of the Schrödinger equation.

Due to its generality the VPA has been applied in various fields [8, 14, 2, 64, 48, 49]. E. g. the scattering of positrons from rare atomic gases has been treated by means of the VPA [8], doubly excited states of He have been described by VPA [14], and the quasi-particle lifetimes in a charged Bose gas and in cuprates have been determined using the VPA [2]. Furthermore, for the calculations of the degree of ionization of a non-degenerate two-dimensional electron-hole plasma, the VPA has been employed [64] to account simultaneously for all bound and unbound states in a screened Coulomb potential. Recently, we utilized the VPA for the description of the scattering and the bound states of metal clusters and fullerenes [48].

Different many-body problems often contain nonlocal potentials (NLP), arising either from the physical aspects of the problem (e.g. energy-dependent potentials), or due to the particular approximation (e.g. in the mean-field treatment). Presence of the NLP essentially complicates the calculations, so that the competition between the reliability of the results and the time expenses becomes an important, if not decisive, question. Therefore the right choice of the calculation procedure or method may become a key question when solving NLP problems. In the present work we propose and develop a new framework for the solution of the NLP problems, based on the VPA. We give the basic concepts of the VPA in Sec. 3.2 and derive the phase-amplitude equations for the NLP in Sec. 3.3. The local version of the equation for the SA and the nonlocal version of the equation for the scattering phase (Eq. 3.2.6) have been already published [6, 20]. In Sec. 3.4 we derive the equation for the scattering amplitude for the NLP and demonstrate how to use this equation for the solution of both the

eigenvalue and the scattering problems. Practical implementation of the solution of the SA equation into the computer codes is performed via the finite-difference scheme (FDS), suggested in Sec. 3.5. The intrinsic property of the FDS applied to VPA is that all calculations require only the diagonal (local) part of the potential, and this does not introduce an approximation as regards the physical content of the problem. Under this condition, the numerical efforts for local and nonlocal problems become comparable. In Sec. 3.5 the numerical errors of the FDS are also discussed.

3.2 Phase-amplitude equations

Consider a spinless particle with energy k^2 in the spherical coordinate system in the presence of the Hermitian ($V(\mathbf{r}, \mathbf{r}') = V(\mathbf{r}', \mathbf{r})$) nonlocal potential [1]:

$$\triangle \Psi(\mathbf{r}) + k^2 \Psi(\mathbf{r}) = \int d\mathbf{r}' V(\mathbf{r}, \mathbf{r}') \Psi(\mathbf{r}') \tag{3.2.1}$$

In the absence of a preferential direction in the system, the potential $V(\mathbf{r}, \mathbf{r}')$ is a function of only the scalar variables r^2, r'^2, $(\mathbf{r}, \mathbf{r}') = rr' \cos \Theta$, and Eq. (3.2.1) admits separation of variables. The radial Schrödinger equation for the radial part $u_\ell(r)$ of the wave function reads

$$\frac{d^2}{dr^2} u_\ell(r) + \left(k^2 - \frac{\ell(\ell+1)}{r^2} \right) u_\ell(r) = \int_0^\infty dr' V_\ell(r, r') u_\ell(r'), \tag{3.2.2}$$

where $V_\ell(r, r') = V_\ell(r', r) = 2\pi rr' \int_{-1}^{1} V_\ell(r, r') P_\ell(\cos \Theta) d(\cos \Theta)$, ℓ is the orbital quantum number.

---

[1] we use units in which $2m = \hbar = e = 1$ throughout

We now introduce new functions $\alpha_\ell(r)$ and $\delta_\ell(r)$ such that:

$$u_\ell(r) = \alpha_\ell(r)[\cos \delta_\ell(r) j_\ell(kr) - \sin \delta_\ell(r) n_\ell(kr)] \equiv \alpha_\ell(r) F_\ell(r), \qquad (3.2.3)$$

and impose the additional condition on the derivative:

$$\frac{d}{dr} u_\ell(r) = \alpha_\ell(r)[\cos \delta_\ell(r) \frac{d}{dr} j_\ell(kr) - \sin \delta_\ell(r) \frac{d}{dr} n_\ell(kr)]. \qquad (3.2.4)$$

Here $j_\ell(kr)$ and $n_\ell(kr)$ are Riccati-Bessel functions defined as regular and irregular solutions of the Schrödinger equation for a free particle. The need of the second condition, Eq. (3.2.4), is clear, since we introduced two functions instead of one. It is straightforward to show that this condition is equivalent to

$$\frac{d\alpha_\ell(r)}{dr} F_\ell(r) = \alpha_\ell(r) \frac{d\delta_\ell(r)}{dr} G_\ell(r), \qquad (3.2.5)$$

where $G_\ell(r) \equiv \sin \delta_\ell(r) j_\ell(kr) + \cos \delta_\ell(r) n_\ell(kr)$. The functions $\delta_\ell(r)$ and $\alpha_\ell(r)$ are conventionally referred to as the *phase* and *wave-amplitude* functions, respectively. They have the following property, which we will refer to as $'additivity'$ property. At each radial position R the values of the functions $\delta_\ell(R)$ and $\alpha_\ell(R)$ have a precise physical meaning: they coincide correspondingly with the partial scattering phase $\widehat{\delta}_\ell^{(R)}$ and with the asymptotic amplitude $\widehat{\alpha}_\ell^{(R)}$ of the wave function of the particle subjected to the potential $V_\ell^{(R)}$ (hat denotes observables). The potential $V_\ell^{(R)}$ is obtained from a cut-off of the potential $V_\ell(r, r')$ at the position R, i.e. $V_\ell^{(R)}(r, r') = V_\ell(r, r') \theta(R-r) \theta(R-r')$, where θ is the step function $\theta(x > 0) = 1$, $\theta(x < 0) = 0$. This property allows a detailed investigation of the accumulation of the phase shift and the asymptotic wave-amplitude due to the structure of the potential. Correspondingly, the asymptotic value of $\delta_\ell(r)$ at $r \longrightarrow \infty$ gives the scattering phase for the genuine potential $V_\ell(r, r')$: $\delta_\ell(\infty) = \widehat{\delta}_\ell$.

Substitution of (3.2.3) and (3.2.5) into (3.2.2) leads[2] to

$$\frac{d\delta_\ell(r)}{dr} = -\frac{F_\ell(r)}{k} \int\limits_0^\infty dr' V_\ell(r,r') F_\ell(r') \exp\left[-\int\limits_{r'}^r \frac{G_\ell(s)}{F_\ell(s)} \cdot \dot\delta_\ell(s) ds\right]. \qquad (3.2.6)$$

Here the upper dot denotes $\frac{d}{ds}$. The initial condition for this equation reads: $\delta_\ell(0) = 0$, corresponding to the absence of the irregular solution at the origin.

Equations (3.2.5) and (3.2.6) represent a system of coupled integro-differential equations, the solution of which allows to restore the wave function using Eq. (3.2.3). Note that the equation for the phase function $\delta_\ell(r)$ does not contain the wave-amplitude function $\alpha_\ell(r)$. This has a profound physical meaning and stems from the fact that the normalization of the wave function is inessential for the scattering and eigenvalue problems. The determining equation for derivative of $\alpha_\ell(r)$, (Eq. (3.2.5)), can be explicitly integrated as soon as $\delta_\ell(r)$ is known:

$$\alpha_\ell(r) = \alpha_\ell(0) \exp\left(\int\limits_0^r \frac{G_\ell(s)}{F_\ell(s)} \cdot \dot\delta_\ell(s) ds\right). \qquad (3.2.7)$$

$\alpha_\ell(0)$ plays the role of the normalization constant of the wave function and is chosen according to the physical content of the problem .

Another useful form of the phase equation is

$$\frac{d\delta_\ell(r)}{dr} = \left(-\frac{1}{k}\right) F_\ell^2(r) \int\limits_0^\infty dr' V_\ell(r,r') \exp\left[-\int\limits_{r'}^r \frac{N_\ell(s)}{F_\ell(s)} ds\right], \qquad (3.2.8)$$

with $N_\ell(s) = \cos\delta_\ell(s) \cdot dj_\ell(ks)/ds - \sin\delta_\ell(r) \cdot dn_\ell(kr)/ds$. It can be readily obtained from the following identity, which will be useful below:

$$dF = Nds - Gd\delta \quad\Rightarrow\quad \int\limits_{r'}^r\left(-\frac{G}{F}d\delta\right) = \int\limits_{r'}^r\left(\frac{dF}{F} - \frac{Nds}{F}\right) = \ln\left(\frac{F(r)}{F(r')}\right) - \int\limits_{r'}^r\frac{N(s)}{F(s)}ds. \quad (3.2.9)$$

---

[2]see Sec. 3.3 for details

3.3 Derivation of the phase-amplitude equations

We start from the Schrödinger equation for the radial wave function u_ℓ :

$$\frac{d^2}{dr^2}u_\ell(r) + \left(k^2 - \frac{\ell(\ell+1)}{r^2}\right)u_\ell(r) = \int\limits_0^\infty dr' V_\ell(r,r')u_\ell(r'), \qquad (3.3.1)$$

and make the replacement $u \to \alpha, \delta$: [3]

$$\begin{cases} u = \alpha F \\ \frac{d\alpha}{dr}F = \alpha\frac{d\delta}{dr}G \end{cases} \quad \text{with} \quad \begin{array}{ll} \alpha \equiv \alpha_\ell(r), \delta \equiv \delta_\ell(r) & \text{new functions} \\ j \equiv j_\ell(kr), n \equiv n_\ell(kr) & \text{Riccati} - \text{Bessel functions} \\ F = j\cos\delta - n\sin\delta & \text{auxiliary} \\ G = j\sin\delta + n\cos\delta & \text{functions} \end{array} \qquad (3.3.2)$$

Using the identity

$$\begin{aligned} \frac{dF}{dr} &= \frac{d}{dr}[j\cos\delta - n\sin\delta] = \left[\frac{dj}{dr}\cos\delta - j\sin\delta\frac{d\delta}{dr} - \frac{dn}{dr}\sin\delta - n\cos\delta\frac{d\delta}{dr}\right] = \\ &= \left[\frac{dj}{dr}\cos\delta - \frac{dn}{dr}\sin\delta\right] - \frac{d\delta}{dr}G, \end{aligned} \qquad (3.3.3)$$

we get the first derivative of u:

$$\frac{du}{dr} = \frac{d(\alpha F)}{dr} = \alpha\frac{dF}{dr} + \frac{d\alpha}{dr}F = \alpha\frac{dF}{dr} + \alpha\frac{d\delta}{dr}G = \alpha\left[\frac{dj}{dr}\cos\delta - \frac{dn}{dr}\sin\delta\right] \qquad (3.3.4)$$

The second derivative of u transforms to:

$$\begin{aligned} \frac{d^2u}{dr^2} &= \frac{d}{dr}\left(\alpha\left[\frac{dj}{dr}\cos\delta - \frac{dn}{dr}\sin\delta\right]\right) = \\ &= \frac{d\alpha}{dr}\left[\frac{dj}{dr}\cos\delta - \frac{dn}{dr}\sin\delta\right] + \alpha\left[\frac{d^2j}{dr^2}\cos\delta - \frac{d^2n}{dr^2}\sin\delta\right] - \\ &\qquad\qquad - \alpha\frac{d\delta}{dr}\left[\frac{dj}{dr}\sin\delta + \frac{dn}{dr}\cos\delta\right] = \end{aligned}$$

---

[3]orbital momentum index is omitted for brevity

$$
= \quad \alpha \frac{d\delta}{dr} \frac{G}{F} \left[\frac{dj}{dr} \cos\delta - \frac{dn}{dr} \sin\delta \right] + \alpha \left[\frac{d^2 j}{dr^2} \cos\delta - \frac{d^2 n}{dr^2} \sin\delta \right] -
$$
$$
-\alpha \frac{d\delta}{dr} \left[\frac{dj}{dr} \sin\delta + \frac{dn}{dr} \cos\delta \right] =
$$
$$
= \quad \alpha \frac{d\delta}{dr} \left(\frac{G}{F} \left[\frac{dj}{dr} \cos\delta - \frac{dn}{dr} \sin\delta \right] - \left[\frac{dj}{dr} \sin\delta + \frac{dn}{dr} \cos\delta \right] \right) +
$$
$$
+\alpha \left[\frac{d^2 j}{dr^2} \cos\delta - \frac{d^2 n}{dr^2} \sin\delta \right] \equiv
$$
$$
\equiv \quad \alpha \frac{d\delta}{dr} \frac{W}{F} + \alpha \left[\frac{d^2 j}{dr^2} \cos\delta - \frac{d^2 n}{dr^2} \sin\delta \right]. \tag{3.3.5}
$$

Let us look at W:

$$
\frac{W}{F} = \quad \frac{G}{F} \left[\frac{dj}{dr} \cos\delta - \frac{dn}{dr} \sin\delta \right] - \left[\frac{dj}{dr} \sin\delta + \frac{dn}{dr} \cos\delta \right] =
$$
$$
= \quad \frac{1}{F} \left(G \cdot \left[\frac{dj}{dr} \cos\delta - \frac{dn}{dr} \sin\delta \right] - F \cdot \left[\frac{dj}{dr} \sin\delta + \frac{dn}{dr} \cos\delta \right] \right) =
$$
$$
= \quad \frac{1}{F} \left(n \frac{dj}{dr} - j \frac{dj}{dr} \right) \left(\cos^2\delta + \sin^2\delta \right). \tag{3.3.6}
$$

Thus, W is a Wronskian of the functions $n(kr)$ and $j(kr)$ and is equal to $-k$:

$$
W = n \frac{dj}{dr} - j \frac{dn}{dr} = -k. \tag{3.3.7}
$$

The substitution of (3.3.5) into the Schrödinger equation gives

$$
-\alpha \frac{d\delta}{dr} \frac{k}{F(\delta(r))} +
$$
$$
+ \left\{ \alpha \left[\frac{d^2 j}{dr^2} \cos\delta - \frac{d^2 n}{dr^2} \sin\delta \right] + \alpha \left(k^2 - \frac{\ell(\ell+1)}{r^2} \right) [j \cos\delta - n \sin\delta] \right\} =
$$
$$
= \int_0^\infty dr' V(r, r)' \alpha(r') F(\delta(r')). \tag{3.3.8}
$$

Expression in the curly brackets, corresponding to the equation for the free particle, is identically zero, and therefore

$$
\frac{d\delta}{dr} = -\frac{F(\delta(r))}{k} \int_0^\infty dr' V(r, r') \frac{\alpha(r')}{\alpha(r)} F(\delta(r')). \tag{3.3.9}
$$

The differential equation for $\alpha(r)$ from the system (3.3.2) may be explicitly integrated when δ is known:

$$\frac{d\alpha}{dr}F(\delta) = \alpha\frac{d\delta}{dr}G(\delta) \quad \Rightarrow \quad \frac{\alpha(r')}{\alpha(r)} = \exp\left(-\int_{r'}^{r} ds\frac{d\delta(s)}{ds}\frac{G(\delta(s))}{F(\delta(s))}\right). \quad (3.3.10)$$

Hence, the equation for $\delta(r)$ has the final form:

$$\frac{d\delta(r)}{dr} = -\frac{1}{k}F(r)\int_{0}^{\infty} dr'V(r,r')F(r')\exp\left[-\int_{r'}^{r}\frac{\delta(s)}{ds}\frac{G(s)}{F(s)}ds\right]. \quad (3.3.11)$$

Substituting $V(r,r') = V(r')\delta(r-r')$ in the Eq. (3.3.11), we obtain the equation, coinciding with the phase equation for the local potential case [21, 7]:

$$\frac{d\delta(r)}{dr} = -\frac{V(r)}{k}F^2(r) = -\frac{V(r)}{k}\left[j\cos(kr)\delta(r) - n(kr)\sin\delta(r)\right]^2. \quad (3.3.12)$$

3.4 Transition to the scattering amplitude representation

In this section we apply the VPA concepts for the derivation of the equation for the scattering amplitude (SA) in the NLP case and show how to use this equation for the solution of both the eigenvalue and the scattering problems.

The relation between the partial SA F_ℓ and the partial scattering phase is well-known [31]: $\mathcal{F}_\ell = \frac{1}{k}\sin\delta_\ell e^{i\delta_\ell}$. According to this, the SA *function*, defined as

$$\mathcal{F}_\ell(r) \equiv \frac{1}{k}\sin\delta_\ell(r)\,e^{i\delta_\ell(r)}, \quad (3.4.1)$$

has the same 'additivity' property, as the wave-amplitude and phase functions in Sec. 3.2: at any point it coincides with the value of the SA for the potential cut off at this point. Now we derive the integro-differential equation for the SA function and

then regularize it in order to make it suitable for the determination of bound state energies in the NLP.

Let us define the auxiliary functions

$$
\begin{aligned}
f(r) &\equiv k\mathcal{F}(r) = e^{i\delta(r)} \cdot \sin\delta(r), \\
\widehat{F}(r) &\equiv F(r)e^{i\delta(r)} = j(kr) + ih^{(1)}(kr)f(r), \\
\widehat{G}(r) &\equiv G(r)e^{i\delta(r)} = n(kr) + h^{(1)}(kr)f(r).
\end{aligned}
\tag{3.4.2}
$$
$$
\tag{3.4.3}
$$

Expressing $\delta(r)$ through $f(r)$, noticing the relation relation between their derivatives

$$
\frac{d\delta(r)}{dr} = \frac{1}{2if(r)+1}\frac{df(r)}{dr},
\tag{3.4.4}
$$

and using the definitions Eq. (3.2.5), we transform the phase equation (3.2.6) to the equation for the function $f(r)$:

$$
\begin{aligned}
\frac{df(r)}{dr} &= \left(-\frac{1}{k}\right)\sqrt{2if(r)+1}\cdot\widehat{F}(r)\cdot\int_0^\infty dr'V(r,r')\frac{\widehat{F}(r')}{\sqrt{2if(r')+1}}\times \\
&\times \exp\left[-\int_{r'}^r \frac{\dot{f}(s)ds}{(2if(s)+1)}\cdot\frac{\widehat{G}(s)}{\widehat{F}(s)}\right],
\end{aligned}
\tag{3.4.5}
$$

with the initial condition $f(0) = 0$. Note that upon transition to the local potential case, Eq. (3.4.5) reduces to the following equation, published in [6, 20]:

$$
\frac{df(r)}{dr} = -\frac{1}{k}\cdot V(r)\widehat{F^2}(r).
\tag{3.4.6}
$$

In terms of the scattering amplitude function, equations for the wave-amplitude function (3.2.7) and for the radial wave function (3.2.3) get the following form:

$$
\alpha_\ell(r) = \alpha_\ell(0)\exp\left(\int_0^r \frac{\widehat{G}_\ell(s)}{\widehat{F}_\ell(s)}\cdot\frac{\dot{f}_\ell(s)ds}{2if_\ell(s)+1}\right),
\tag{3.4.7}
$$

$$u_\ell(r) = \alpha_\ell(r)\frac{\widehat{F}_\ell(r)}{\sqrt{2if_\ell(s)+1}}. \tag{3.4.8}$$

In the complex plane of the wavevector k each partial SA describes stationary and quasi-stationary states characterized by a certain orbital momentum ℓ. When SA has a pole on the positive imaginary semi-axis ($k = i\kappa_n$, $\kappa_n \in \Re > 0$), then this value of k corresponds to the energy of the stationary state in the discrete spectrum: $E_n = (i\kappa_n)^2 < 0$.

The condition, from which the bound state energy can be determined, reads:

$$f(\infty; \kappa_n) = \infty. \tag{3.4.9}$$

The pole of the scattering amplitude for the complex wavevector corresponds to the quasibound state with a finite lifetime, for example, the wave penetrating through the potential barrier. For the real positive values of the wavevector the SA function describes the scattering states.

Thus, all quantum-mechanical problems are reformulated in the VPA as follows:

• The bound state energies are defined by the solution of a single equation for the SA function, Eq. (3.4.13);

• The wave function of the particle may be found from equations (3.4.7) and (3.4.8).

Now we want to adapt Eq. (3.4.5) for the eigenvalue problems. We rewrite it for $k = i\kappa$, $\kappa > 0$. The Riccati-Bessel functions of the imaginary argument can be expressed through the modified Riccati-Bessel functions of the real argument $p_\ell(\kappa r)$ and $q_\ell(\kappa r)$ [1]:

$$j_\ell(i\kappa r) = \beta p_\ell(\kappa r); n_\ell(i\kappa r) = \frac{i}{\beta}\left[\beta^2 p_\ell(\kappa r) - q_\ell(\kappa r)\right]; h_\ell^{(1)}(i\kappa r) = \frac{1}{\beta}q_\ell(\kappa r) \tag{3.4.10}$$

with $\beta = (i)^{\ell+1}$. Then the integrand in the last line of Eq. (3.4.5) becomes:

$$\frac{df(s)}{2if(s)+1} \cdot \frac{\hat{G}(s)}{\hat{F}(s)} = \frac{df(s)}{2if(s)+1} \cdot \frac{i\left[\beta^2 p(\kappa s) - q(\kappa s)\left(if(s)+1\right)\right]}{\left[\beta^2 p(\kappa s) + q(\kappa s)\left(if(s)\right)\right]} =$$

$$= \frac{1}{2} \cdot \frac{d(2if(s)+1)}{2if(s)+1} - \frac{q(\kappa s) \cdot d\left(if(s)\right)}{q(\kappa s) \cdot if(s) + \beta^2 p(\kappa s)}. \quad (3.4.11)$$

The integration of the first term gives:

$$\exp\left(-\frac{1}{2}\ln\left[\frac{2if(r)+1}{2if(r')+1}\right]\right) = \frac{\sqrt{2if(r')+1}}{\sqrt{2if(r)+1}}, \quad (3.4.12)$$

which cancels the the analogous square roots in the first line of Eq. (3.4.5). Finally, using the identity (3.2.9) we obtain the integro-differential equation for the function $if(r)$:

$$\frac{d(if(r))}{dr} = -\frac{2}{\beta^2\kappa}\left[if(r)q(\kappa r) + \beta^2 p(\kappa r)\right]^2 \times$$

$$\times \int_0^r dr' V(r,r') \cosh\left\{-\int_{r'}^r ds \frac{if(s)\dot{q}(\kappa s) + \beta^2 \dot{p}(\kappa s)}{if(s)q(\kappa s) + \beta^2 p(\kappa s)}\right\}. \quad (3.4.13)$$

The coefficient 2 and the finite upper limit of the external integral on the right-hand side of (3.4.13) originate from the symmetrization of the integrand with respect to the interchange of r and r'. After the substitution $if(r) \equiv \beta^2 y(r)$ Eq. (3.4.13) is transformed to an equation for the *real* function $y(r)$:

$$\frac{dy(r)}{dr} = -\frac{2}{\kappa}\left[y(r)q(\kappa r) + p(\kappa r)\right]^2 \times$$

$$\times \int_0^r dr' V(r,r') \cosh\left\{-\int_{r'}^r ds \frac{y(s)\dot{q}(\kappa s) + \dot{p}(\kappa s)}{y(s)q(\kappa s) + p(\kappa s)}\right\}. \quad (3.4.14)$$

Since $V(r,r')$ is assumed Hermitian and the functions $p_\ell(\kappa r)$ and $q_\ell(\kappa r)$ are real, the initial condition $y_\ell(0,\kappa) = 0$ implies that $y_\ell(r,\kappa)$ is real everywhere. Bound state exists at the eigenvalue $E = -\kappa^2$ when $y_\ell(\infty,\kappa)$ has a pole.

The regularization of Eq. (3.4.14) can be made in two different ways: 1. By introducing an inverse function $y = 1/\phi$, or 2. Using a tangent function $y = \tan\gamma$. The first option yields the equation:

$$
\begin{aligned}
\frac{d\phi(r)}{dr} &= \frac{2}{\kappa}[q(\kappa r) + \phi(r)p(\kappa r)]^2 \times \\
&\times \int_0^r dr'V(r,r')\cosh\left\{-\int_{r'}^r ds\frac{\dot{q}(\kappa s) + \phi(s)\dot{p}(\kappa s)}{q(\kappa s) + \phi(s)p(\kappa s)}\right\}.
\end{aligned}
\qquad (3.4.15)
$$

Then the eigenvalue problem reduces to finding the zeros of $\phi_\ell(\infty, \kappa)$.

In the second case we obtain an equation with the initial condition $\gamma_\ell(0, \kappa) = 0$

$$
\begin{aligned}
\frac{d\gamma(r)}{dr} &= -\frac{2}{\kappa}[q(\kappa r)\sin\gamma(r) + p(\kappa r)\cos\gamma(r)]^2 \times \\
&\times \int_0^r dr'V(r,r')\cosh\left\{-\int_{r'}^r ds\frac{\sin\gamma(s)\dot{q}(\kappa s) + \cos\gamma(s)\dot{p}(\kappa s)}{\sin\gamma(s)q(\kappa s) + \cos\gamma(s)p(\kappa s)}\right\}
\end{aligned}
\quad (3.4.16)
$$

The condition for the bound state is $\gamma_\ell(\infty, \kappa) = (2n + 1)\pi/2$, $n \in Z$. It is useful to note that the sign of the derivatives of the functions $\delta_\ell(r)$, $y_\ell(r)$, $\phi_\ell(r)$, $\gamma_\ell(r)$, as can be seen from the equations (3.2.8), (3.4.14 – 3.4.16), is fully specified by the sign of the potential $V_\ell(r, r')$.

To illustrate the method we calculate the scattering amplitude function for zero orbital momentum ($\ell = 0$). Consider a neutral atom and a negative hydrogen ion as simple physical systems.

In Fig. 3.1 the physical meaning of the function $\gamma_0(r) = \arctan(\kappa\mathcal{F}_0(r))$ is illustrated for the attractive Coulomb potential for particle with the energy $E = -0.0556$ Hartree. The integration of the Eq. (3.4.16) (together with the initial condition this equation forms Cauchy problem) is perfomed from $r = 0$ to $r = \infty$. The original potential $V(r) = -1/r$ is nonzero everywhere (see upper plot) and affects the derivative
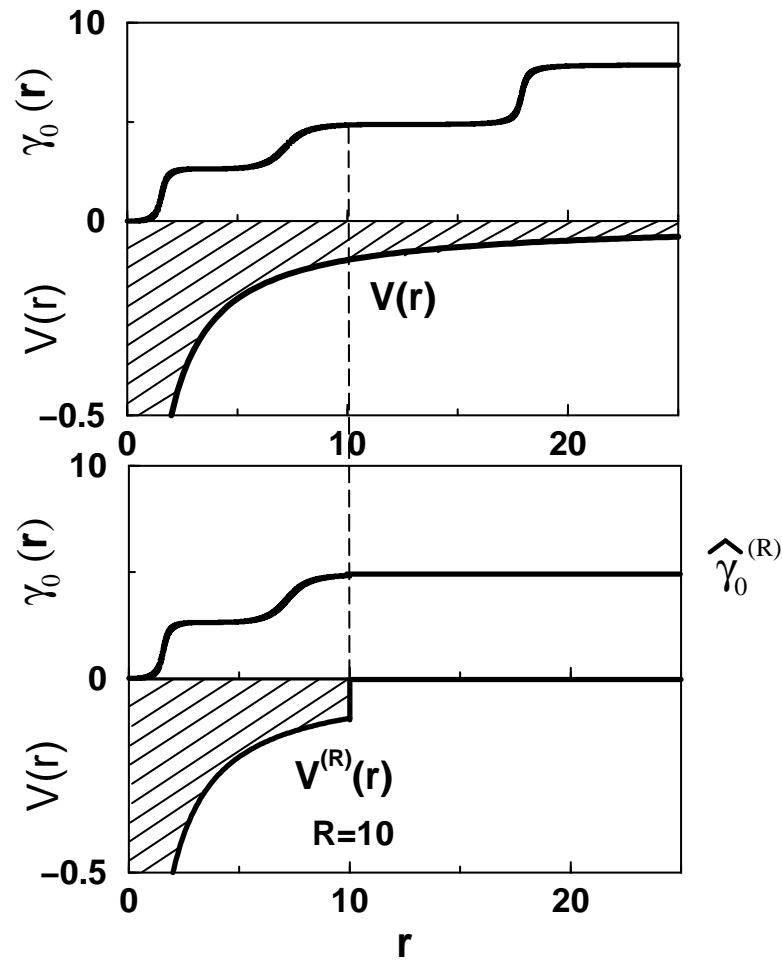
Figure 3.1: The behavior of arctangent of the scattering amplitude function $\gamma_0(r)$ built for the Coulomb potential $V(r) = -1/r$ (upper plot) and for the Coulomb cut-off at $R = 10$ (lower plot). At the radial distance R the value of $\gamma_0(r = R)$ coincides with arctangent of the scattering amplitude $\widehat{\gamma_0}^{(R)} = \arctan(\kappa \widehat{\mathcal{F}_0}^{(R)})$, associated with cut-off potential $V^{(R)}(r)$.

of $\gamma_0(r)$ along the whole radial axis. The asymptotic value of the arctangent of the SA function gives the arctangent of the scattering amplitude: $\gamma_0(\infty) = \widehat{\gamma}_0 = \arctan \widehat{\mathcal{F}_0}$. For the potential cut-off at R, the value of the derivative of $\gamma_0(r)$ is zero from R to ∞, and the value of the function $\gamma_0(r)$ coincides with the asymptotic value $\widehat{\gamma}_0^{(R)} \equiv \gamma_0(\infty) = \gamma_0(R)$ (see lower plot).
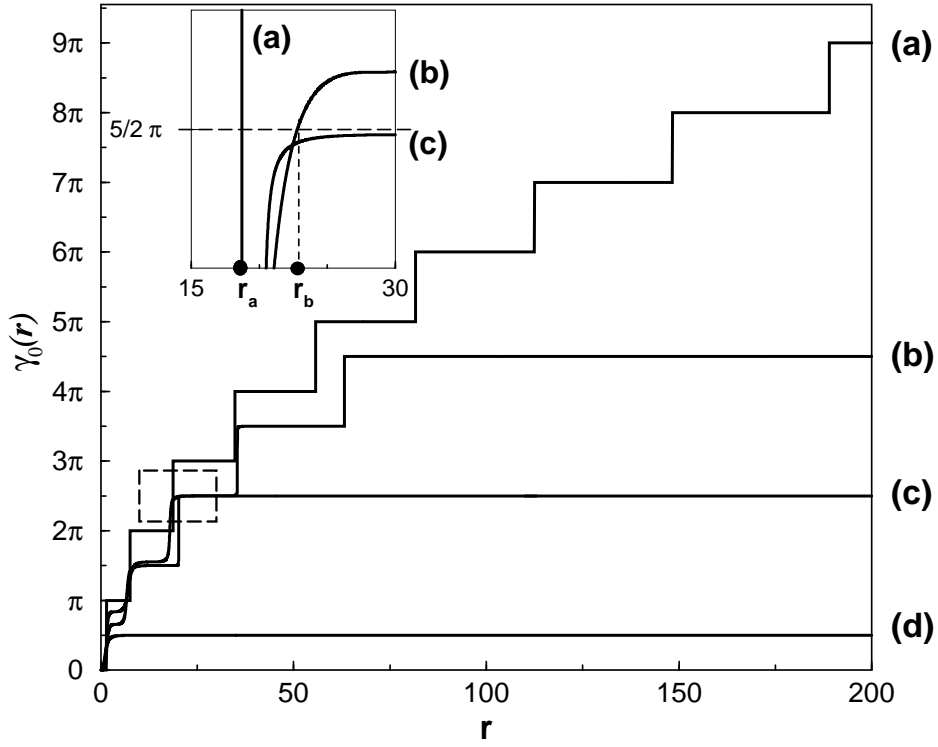
Figure 3.2: Function $\gamma_0(r)$ for different negative energies for the attractive Coulomb potential. (a) $E = -0.5 \times 10^{-10}$, (b) $E = -0.01$, (c) $E = -0.0556$, (d) $E = -0.5$ (energies are given in Hartree). Inset: the behavior of $\gamma_0(r)$ in the vicinity of $\gamma_0(r) = \frac{5}{2}\pi$.

The behavior of $\gamma_0(r)$ for the different energies (plots (a)–(d)) is shown in Fig. 3.2. The ns-eigenstate with a given energy appears when the value of the function $\gamma_0(r)$ becomes equal to $(n - 1/2)\pi$. If it happens at a finite distance R, then this eigenstate is associated with the cut-off potential $V^{(R)}$. If this distance is infinite the eigenstate

corresponds to a genuine potential. The blow-up of the vicinity of $\gamma_0(r) = \frac{5}{2}\pi$ is depicted in the inset: in cases (a) and (b) the eigenstate arises at the finite distance $r_a(r_b)$; in case (c) γ_0 will reach $\frac{5}{2}\pi$ at the infinity (therefore E_c is the energy of the 3s-state of the original Coulomb potential); the energy E_d will never be the 3s-eigenenergy of any (cut-off or genuine) Coulomb potential. Indeed, E_d is a ground state energy of the latter and $\gamma_0(r, E_d)$ reaches the value $\pi/2$ at the infinity.

3.5   Finite-difference scheme.

The main difference between the numerical treatments of the local and the nonlocal potential is that, instead of an ordinary differential equation (c.f. (3.4.6)) in the first case, one has to deal with the integro-differential equation (c.f. (3.4.15) or (3.4.16)). For concreteness, let us consider Eq. (3.4.16). While for local potentials rather fast, well-known methods (e.g. Runge-Kutta method) can be applied, for nonlocal potentials one has to perform two additional integrations at each step of the calculations of the derivatives. Evidently, the numerical efforts grow substantially with the total number of mesh points used for the representation of the desired function, moreover, it quickly grow together with the order number of a mesh point inside the same mesh.

In this section we suggest an algorithm for the numerical solution of the first-kind Volterra integro-differential equation. The essence of our algorithm is based on the '*additivity*' property of the function $\gamma(r)$: For a given set of mesh points $(r_1 = 0,\ ...,\ r_n = r,\ r_{n+1} = r + \delta r,\ ...)$ for the calculation of $\gamma_{n+1} = \gamma(r + \delta r)$ one needs to integrate over all values of γ, calculated at the previous n points. It is this integration which comprises the main difficulty of the numerical solution and makes the main difference to the local potential case. We develop an approximate scheme,

in which the calculation of the $(n + 1)$-th point requires only the information, stored on the n-th step, *and* few additional algebraic operations.

We start by considering the integrals of Eq. (3.4.16) of the following form

$$J[r] \equiv \int\limits_0^r dr' V_\ell(r, r') \, \exp\left\{ - \int\limits_{r'}^r Q(s)ds \right\}, \qquad (3.5.1)$$

and

$$J[r + \delta r] \equiv \int\limits_0^{r+\delta r} dr' V_\ell(r + \delta r, r') \, \exp\left\{ - \int\limits_{r'}^{r+\delta r} Q(s)ds \right\}, \qquad (3.5.2)$$

where

$$Q(s) = \frac{\sin\gamma(s)\dot{q}(\kappa s) + \cos\gamma(s)\dot{p}(\kappa s)}{\sin\gamma(s)q(\kappa s) + \cos\gamma(s)p(\kappa s)}. \qquad (3.5.3)$$

Our aim is to express $J[r + \delta r]$ through $J[r]$, r and δr. For the numerical estimation of the integrals below we will use the rectangular scheme with an arbitrary mesh, which gives the integral value with the numerical error of the 2-nd order in δr:

$$\int\limits_{r_1}^{r_N} f(r)dr = (f_1 + f_2 + ... + f_{N-1})\delta r + \max_{x \in [r_1, r_N]} |f'(x)| \frac{(N-1)(\delta r)^2}{2}. \qquad (3.5.4)$$

The simplicity of the rectangular scheme, without loss of generality, allows to clear the calculation procedure, described below. Of course, application of the higher order integration schemes will increase the accuracy of this procedure.

For the exponent from (3.5.2) we write

$$\exp\left\{ - \int\limits_{r'}^{r+\delta r} Q(s)ds \right\} = \exp\left\{ - \int\limits_{r'}^{r} Q(s)ds \right\} \exp\left\{ - \int\limits_{r}^{r+\delta r} Q(s)ds \right\}.$$

The last factor does not contain r' and is equal to

$$\exp\left(-Q(r)\delta r + \max_{x \in [r, r+\delta r]} | - \dot{Q}(x)| \frac{(\delta r)^2}{2} \right) =$$

$$= \exp\left(-Q(r)\delta r \right) \left(1 + \max_{x \in [r, r+\delta r]} |\dot{Q}(x)| \frac{(\delta r)^2}{2} + ... \right).$$

Hence, the target integral (3.5.2) approximately equals

$$J[r + \delta r] \simeq \exp(-Q(r)\delta r) \int_0^{r+\delta r} dr' V(r + \delta r, r') \exp\left\{ -\int_{r'}^{r} Q(s)ds \right\}. \qquad (3.5.5)$$

with the upper value of the 2-nd order error R_{exp}

$$R_{\exp} \leq \max_{x \in [r,r+\delta r]} |Q'(x)| \frac{(\delta r)^2}{2} \times \max_{x \in [0,r+\delta r]} |J(x)| \qquad (3.5.6)$$

In the same way the integral in Eq. (3.5.5) can be divided into two parts

$$\int_0^r dr' V(r + \delta r, r') \exp\left\{ -\int_{r'}^{r} Q(s)ds \right\} +$$

$$+ \int_r^{r+\delta r} dr' V(r + \delta r, r') \exp\left\{ -\int_{r'}^{r} Q(s)ds \right\}. \qquad (3.5.7)$$

The second term of this expression is approximated up to the error R_{int}

$$R_{int} \leq \max_{x \in [r,r+\delta r]} \left| \frac{\partial V(r + \delta r, x)}{\partial x} \right| \frac{(\delta r)^2}{2} \qquad (3.5.8)$$

by

$$\int_r^{r+\delta r} dr' V(r + \delta r, r') \exp\left\{ -\int_{r'}^{r} Q(s)ds \right\} \simeq$$

$$\simeq \delta r V(r + \delta r, r + \delta r) \exp\left\{ -\int_{r+\delta r}^{r} Q(s)ds \right\} =$$

$$= \delta r\ V(r + \delta r, r + \delta r) \exp(Q(r)\delta r). \qquad (3.5.9)$$

The first term of Eq. (3.5.7)

$$\int_0^r dr' V(r + \delta r, r') \exp\left\{ -\int_{r'}^{r} Q(s)ds \right\} \qquad (3.5.10)$$

differs from $J[r]$ only in that the potential V is evaluated at the point $(r + \delta r, r')$ instead of (r, r'). Therefore, we can proceed in two different ways.

- The expansion of $V(r + \delta r)$ in Taylor series yields

$$V(r + \delta r, r') \simeq V(r, r') + \frac{\partial V(r, r')}{\partial r} \delta r + \frac{1}{2} \frac{\partial^2 V(r, r')}{\partial r^2} \delta r^2 + \cdots . \qquad (3.5.11)$$

The first terms yields the following approximate expression for $J[r + \delta r]$

$$J[r + \delta r] \simeq J[r] \, e^{-Q(r)\delta r} + V(r + \delta r, r + \delta r)\delta r. \qquad (3.5.12)$$

For the complete account of all first-order in δr terms for $J[r + \delta r]$ it is necessary to estimate the term with the first derivative of the potential

$$J^{(1)}[r] \equiv \int\limits_0^r dr' \, \frac{\partial V(r, r')}{\partial r} \exp\left(-\int\limits_{r'}^r Q(s)ds\right). \qquad (3.5.13)$$

This integral can be treated, in the same way as previously described in Eqs. (3.5.1 – 3.5.12), by calculation of increments. For the term containing the first derivative we obtain

$$J^{(1)}[r] \simeq J^{(1)}[r - \delta r]e^{-Q(r-\delta r)\delta r} + \left.\frac{\partial V(x, y)}{\partial x}\right|_{x,y=r} \delta r; \qquad (3.5.14)$$

$$\begin{aligned} J[r + \delta r] \simeq{}& J[r]e^{-Q(r)\delta r} + V(r + \delta r, r + \delta r)\delta r + \\ &+ J^{(1)}[r - \delta r]e^{-(Q(r-\delta r)+Q(r))\delta r}\delta r + \left.\frac{\partial V(x, y)}{\partial x}\right|_{x,y=r} e^{-Q(r)\delta r}\delta r^2. \end{aligned} \quad (3.5.15)$$

In terms of finite differences we write

$$J_{n+1} \simeq J_n \, e^{-Q_n \Delta r_n} + \left(V_{n+1,n+1} + J^{(1)}_{n-1}e^{-(Q_{n-1}+Q_n)\Delta r_n}\right)\Delta r_n, \; \Delta r_n = r_{n+1} - r_n. \, (3.5.16)$$

As can be seen from the structure of the equations (3.5.12), (3.5.15), only the diagonal parts of the nonlocal potential $- V(r, r)$ and $\left.\frac{\partial V(x,y)}{\partial x}\right|_{x,y=r}$ $-$ enter all FDS expressions.

This *locality* is a principal property of the FDS, which arises from the Taylor expansion of the potential $V(r + \delta r, r')$ in the vicinity of r. Whereas the 'localization' of the potential in the traditional HF treatments introduces an approximation and often reduces the physical quality of the problem, in the present approach the locality of the potential is intrinsic *inapproximate* property of the FDS applied to the VPA equations.

Accounting for terms in the potential expansion up to those containing the 1-st derivative implies an accuracy of the calculation of $J[r + \delta r]$ of the 1-st order in δr with the numerical error of the second order.

• The second way is useful when the potential is a product of two parts, separately depending on r and r': $V(r, r') = U(r)\,W(r')$. In this case the finite-difference scheme becomes exact (in the second order in δr), since we can write

$$J_{n+1} = \frac{U_{n+1}}{U_n} J_n \, \exp(-Q_n \Delta r_n) + U_{n+1} W_{n+1} \Delta r_n. \qquad (3.5.17)$$

We conclude this part by noting the features of the finite-difference scheme based on Eq. (3.5.16) or on Eq. (3.5.17):

i) It has a simple form;

ii) At each step it reduces the integration to the evaluation of the potential at the last point ($V_{n+1,n+1}$ in Eq. (3.5.16) with all the other data stored at the previous n and $n-1$ steps;

iii) The dependence on only the diagonal in r and r' part of $V(r, r')$ significantly simplifies the calculations;

iv) It can be directly used for the numerical implementation and built into the standard packages of the numerical solution of the ordinary differential equations. This FDS corresponds to the 1-st order integration method, but basing on the same idea

it can be easily generalized to the next order methods with the higher integration accuracies.

3.6   Conclusions

Traditional treatments of the eigenstate problem for the nonlocal potential imply the expansion over the basis set. In this chapter, based on the Variable Phase approach we proposed a new method that avoids the basis-set expansion ansatz by the solution of a first-order Volterra integro-differential equation. Therefore the method is independent of the choice of the basis. Furthermore, we proposed a fast numerical scheme for the numerical solution of such integro-differential equations and demonstrated that the algorithm involves numerical efforts that are of the same order as those required for the local potential case.

Chapter 4

Hartree-Fock approximation within the variable phase approach

Based on the results of the previous chapter, we reformulate the Hartree-Fock approach in the VPA language (Sec. 4.1). The feature and the advantage of this treatment is that for the numerical solution of the HF equation only the diagonal part of the nonlocal HF potentials is required (Sec. 4.2). This is an essential improvement in the calculational efforts and it does not imply any additional approximation.

4.1   VPA equations of the HF problem

The Hartree-Fock single-electron wave functions $\Psi_i(\mathbf{r}_i)$ are the self-consistent solutions of the HF system of coupled equations

$$\begin{cases} -\triangle \Psi_i(\mathbf{r_i}) + V^{ion}(\mathbf{r_i}) - k_i^2 \Psi_i(\mathbf{r_i}) = \\ \\ = -\sum_{k \neq i} \int d^3\mathbf{r}' \frac{\Psi_k^*(\mathbf{r}')\Psi_k(\mathbf{r}') - \Psi_k^*(\mathbf{r}')\Psi_k(\mathbf{r}_i)}{|\mathbf{r}_i - \mathbf{r}'|} \Psi_i(\mathbf{r}') \end{cases} \Bigg|_{i=1..n} \qquad (4.1.1)$$

where the left-hand side of i-th equation is the Hamilton operator of the i-th electron in the local ionic field V^{ion}, the right-hand side corresponds to the nonlocal interaction with the field of other electrons of the system.

In the terms of the VPA, each wave function $\Psi_{\varepsilon\ell\mu}(\mathbf{r}_i)$ characterized by the quantum numbers $(\varepsilon\ell\mu)$ is related to the corresponding scattering-amplitude and wave-amplitude functions $f_{\varepsilon\ell}(r)$ and $\alpha_{\varepsilon\ell}(r)$ by

$$\Psi_{\varepsilon\ell\mu}(\mathbf{r}) = \frac{u_{\varepsilon\ell}(r)}{r} \, Y_{\ell\mu}(\theta, \phi) = \frac{\alpha_{\varepsilon\ell}(r)\widehat{F}_{\varepsilon\ell}(r)}{r\sqrt{2if_{\varepsilon\ell}(r)+1}} \, Y_{\ell\mu}(\theta, \phi), \tag{4.1.2}$$

$$\widehat{F}_{\varepsilon\ell}(r) = j_\ell(kr) + ih_\ell^{(1)}(kr)f_{\varepsilon\ell}(r); \quad \widehat{N}_{\varepsilon\ell}(r) = \frac{dj_\ell(kr)}{dr} + i\frac{dh_\ell^{(1)}(kr)}{dr}f_{\varepsilon\ell}(r). \tag{4.1.3}$$

The system of the coupled integro-differential equations on the functions $\alpha_{\varepsilon\ell}(r)$ and $f_{\varepsilon\ell}(r)$, corresponding to the Hartree-Fock system, has the form (c.f. Eqs. 3.4.7, 3.4.13)

$$\begin{cases} i\dot{f}_{\ell_1}(r_1) = -\frac{2}{k_1}\widehat{F}_{\ell_1}^2(r_1)\left[V_{\ell_1}^{ion}(r_1) + \int\limits_0^{r_1} dr_1' V_{\ell_1}(r_1, r_1')\exp\left(-\int\limits_{r_1'}^{r_1}\frac{\widehat{N}_{\ell_1}(s_1)}{\widehat{F}_{\ell_1}(s_1)}ds_1\right)\right] \\ \alpha_{\ell_1}(r_1) = \alpha_{\ell_1}(0)\exp\left(\int\limits_0^{r_1}\frac{\widehat{G}_{\ell_1}(s_1)}{\widehat{F}_{\ell_1}(s_1)} \cdot \frac{\dot{f}_{\ell_1}(s_1)ds_1}{2if_{\ell_1}(s_1)+1}\right) \\ \dots \\ i\dot{f}_{\ell_n}(r_n) = -\frac{2}{k_n}\widehat{F}_{\ell_n}^2(r_n)\left[V_{\ell_n}^{ion}(r_n) + \int\limits_0^{r_n} dr_n' V_{\ell_n}(r_n, r_n')\exp\left(-\int\limits_{r_n'}^{r_n}\frac{\widehat{N}_{\ell_n}(s_n)}{\widehat{F}_{\ell_n}(s_n)}ds_n\right)\right] \\ \alpha_{\ell_n}(r_n) = \alpha_{\ell_n}(0)\exp\left(\int\limits_0^{r_n}\frac{\widehat{G}_{\ell_n}(s_n)}{\widehat{F}_{\ell_n}(s_n)} \cdot \frac{\dot{f}_{\ell_n}(s_n)ds_n}{2if_{\ell_n}(s_n)+1}\right). \end{cases} \tag{4.1.4}$$

Initial conditions for $2n$ unknown functions are chosen as: $f_{\ell_i}(0) = 0$, $\alpha_{\ell_i}(0) = 1$, $i = 1 \dots n$. The coupling between the equations is incorporated into the HF potentials $V_{\ell_i}(r_i, r_i')$.

4.2 The Hartree-Fock potential

The mean-field potential of the Hartree-Fock problem[1] provides an example of a nonlocal potential, namely

$$V(\mathbf{r}, \mathbf{r}') = \sum_{\varepsilon\ell\mu} \frac{\Psi_{\varepsilon\ell\mu}^*(\mathbf{r}')\Psi_{\varepsilon\ell\mu}(\mathbf{r}') - \Psi_{\varepsilon\ell\mu}^*(\mathbf{r}')\Psi_{\varepsilon\ell\mu}(\mathbf{r})}{|\mathbf{r} - \mathbf{r}'|}. \tag{4.2.1}$$

---

[1]see, for example, [5] Eq. (17.15), p.333

It's ℓ-th orbital part [19] is determined by

$$V_\ell(r, r') = 2\pi rr' \int\limits_{-1}^{1} V(\mathbf{r}, \mathbf{r}') P_\ell(x) dx, \qquad \text{with} \quad x = \cos\Theta, \qquad (4.2.2)$$

Θ is the angle between $\mathbf{r}$ and $\mathbf{r}'$ and $\cos\Theta = \cos\theta\cos\theta' + \sin\theta\sin\theta'\cos(\phi - \phi')$.

Now we want to use the property of the finite-difference scheme (FDS), discussed in Sec. 3.5. According to the FDS, it is sufficient to consider only the diagonal (in r and r') part of the potential $V(r, r')$ (c.f. Eq. 3.5.15). For this purpose we will find the diagonal parts of the Hartree and Fock terms.

First, the Slater expansion of the inter-electron Coulomb repulsion in terms of the Legendre polynomials has the form [2]:

$$\frac{1}{|\mathbf{r} - \mathbf{r}'|} = \sum_{\lambda=0}^{\infty} \frac{1}{r} \left(\frac{r'}{r}\right)^\lambda P_\lambda(x) \qquad (4.2.3)$$

We assume that all orbital shells of the system are closed, that is equivalent to imposing the spherical symmetry on the system. Then, the Hartree and the Fock potentials read:

$$
\begin{aligned}
V^H(\mathbf{r}, \mathbf{r}') &= \sum_{\varepsilon\ \alpha\ \beta} \frac{\Psi^*_{\varepsilon\alpha\beta}(\mathbf{r}')\Psi_{\varepsilon\alpha\beta}(\mathbf{r}')}{|\mathbf{r} - \mathbf{r}'|} = \\
&= \sum_{\varepsilon\ \alpha\ \beta} \frac{u^2_{\varepsilon\alpha}(r')}{(r')^2} \, |Y_{\alpha\beta}(\theta', \varphi')|^2 \cdot \sum_{\lambda=0}^{\infty} \frac{1}{r}\left(\frac{r'}{r}\right)^\lambda P_\lambda(x),
\end{aligned} \qquad (4.2.4)
$$

$$
\begin{aligned}
V^F(\mathbf{r}, \mathbf{r}') &= \sum_{\varepsilon\ \alpha\ \beta} \frac{\Psi^*_{\varepsilon\alpha\beta}(\mathbf{r}')\Psi_{\varepsilon\alpha\beta}(\mathbf{r})}{|\mathbf{r} - \mathbf{r}'|} = \\
&= \sum_{\varepsilon\ \alpha\ \beta} \frac{u_{\varepsilon\alpha}(r')u_{\varepsilon\alpha}(r)}{rr'} \, Y^*_{\alpha\beta}(\theta', \varphi')Y_{\alpha\beta}(\theta, \varphi) \cdot \sum_{\lambda=0}^{\infty} \frac{1}{r}\left(\frac{r'}{r}\right)^\lambda P_\lambda(x).
\end{aligned} \qquad (4.2.5)
$$

---

[2] in [87] see Eq. 5.17.4.(21), p.165 and Eq. 5.17.2.(9), the product definition can be found in [10], Eq. (5.16.1)

Using the known sum rules[3]:

$$\sum_{\beta} |Y_{\alpha\beta}(\theta, \varphi)|^2 = \frac{2\alpha + 1}{4\pi}, \tag{4.2.6}$$

$$\sum_{\beta} Y_{\alpha\beta}^*(\theta', \varphi') Y_{\alpha\beta}(\theta, \varphi) = \frac{2\alpha + 1}{4\pi} P_\alpha(x), \tag{4.2.7}$$

the potentials are transformed to

$$V^H(\mathbf{r}, \mathbf{r}') = \sum_{\varepsilon\,\alpha} \frac{u_{\varepsilon\alpha}^2(r')}{(r')^2} \frac{2\alpha + 1}{4\pi} \sum_{\lambda=0}^{\infty} \frac{1}{r} \left(\frac{r'}{r}\right)^\lambda P_\lambda(x), \tag{4.2.8}$$

$$V^F(\mathbf{r}, \mathbf{r}') = \sum_{\varepsilon\,\alpha} \frac{u_{\varepsilon\alpha}(r') u_{\varepsilon\alpha}(r)}{rr'} \frac{2\alpha + 1}{4\pi} P_\alpha(x) \sum_{\lambda=0}^{\infty} \frac{1}{r} \left(\frac{r'}{r}\right)^\lambda P_\lambda(x), \tag{4.2.9}$$

and their ℓ-th orbital parts take the form:

$$V_\ell^H(r, r') = \sum_{\varepsilon\,\alpha} \frac{2\alpha + 1}{2} \frac{u_{\varepsilon\alpha}^2(r')}{r'} \sum_{\lambda=0}^{\infty} \left(\frac{r'}{r}\right)^\lambda \int_{-1}^{1} P_\lambda(x) P_\ell(x) dx, \tag{4.2.10}$$

$$V_\ell^F(r, r') = \sum_{\varepsilon\,\alpha} u_{\varepsilon\alpha}(r') u_{\varepsilon\alpha}(r) \frac{2\alpha + 1}{2} \sum_{\lambda=0}^{\infty} \frac{1}{r} \left(\frac{r'}{r}\right)^\lambda \int_{-1}^{1} P_\alpha(x) P_\lambda(x) P_\ell(x) dx. \tag{4.2.11}$$

Integrals of two[4] and three[5] Legendre polynomials

$$\int_{-1}^{1} P_\lambda(x) P_\ell(x) dx = \frac{2\delta_{\lambda\ell}}{\sqrt{(2\lambda + 1)(2\ell + 1)}}, \tag{4.2.12}$$

$$\int_{-1}^{1} P_\alpha(x) P_\lambda(x) P_\ell(x) dx = 2 \begin{pmatrix} \alpha & \lambda & \ell \\ 0 & 0 & 0 \end{pmatrix}^2 = \frac{2}{2\ell + 1} \left(C_{\alpha 0 \lambda 0}^{\ell 0}\right)^2 \tag{4.2.13}$$

---

[3]in [87]: Eq. 5.10.1.(1), p.150; Eq. 5.17.2.(9) together with 5.16.1.(10)
[4]in [87]: Eq. 5.9.3.(10)
[5]in [87]: Eq. 5.9.(5); Eq. 8.1.2.(11)

reduce Eq. (4.2.10) and (4.2.11) to

$$V_\ell^H(r, r') = \sum_{\varepsilon \ \alpha} \frac{2\alpha + 1}{2\ell + 1} \frac{u_{\varepsilon\alpha}^2(r')}{r'} \left(\frac{r'}{r}\right)^\ell \qquad (4.2.14)$$

$$V_\ell^F(r, r') = \sum_{\varepsilon \ \alpha} \frac{2\alpha + 1}{2\ell + 1} \frac{u_{\varepsilon\alpha}(r')u_{\varepsilon\alpha}(r)}{r} \sum_{\lambda=0}^\infty \left(\frac{r'}{r}\right)^\lambda \left(C_{\alpha 0 \lambda 0}^{\ell 0}\right)^2. \qquad (4.2.15)$$

Their diagonal in r and r' parts amount to

$$V_\ell^H(r, \ r) = V_\ell^H(r, \ r' = r) = \sum_{\varepsilon \ \alpha} \frac{2\alpha + 1}{2\ell + 1} \frac{u_{\varepsilon\alpha}^2(r)}{r}, \qquad (4.2.16)$$

$$V_\ell^F(r, \ r) = V_\ell^F(r, \ r' = r) = \sum_{\varepsilon \ \alpha} \frac{2\alpha + 1}{2\ell + 1} \frac{u_{\varepsilon\alpha}^2(r)}{r} \sum_{\lambda=0}^\infty \left(C_{\alpha 0 \lambda 0}^{\ell 0}\right)^2, \qquad (4.2.17)$$

$$V_\ell^H(r, \ r) - V_\ell^F(r, \ r) = \sum_{\varepsilon \ \alpha} \frac{2\alpha + 1}{2\ell + 1} \frac{u_{\varepsilon\alpha}^2(r)}{r} \left(1 - \sum_{\lambda=0}^\infty \left(C_{\alpha 0 \lambda 0}^{\ell 0}\right)^2\right). \qquad (4.2.18)$$

Using the expressions for the Clebsh-Gordan coefficients for $\ell = \alpha + \lambda > \alpha$ [6]

$$C_{\alpha 0 \ \lambda 0}^{\alpha+\lambda 0} = \frac{(\alpha + \lambda)!}{\alpha!\lambda!}\sqrt{\frac{(2\alpha)!(2\lambda)!}{(2\alpha + 2\lambda)!}} = \frac{\ell!}{\alpha!(\ell - \alpha)!}\sqrt{\frac{(2\alpha)!(2\ell - 2\alpha)!}{(2\ell)!}}, \qquad (4.2.19)$$

and for $\ell = \alpha - \lambda < \alpha$ [7]

$$C_{\alpha 0 \ \lambda 0}^{\alpha-\lambda 0} = \frac{(-1)^\lambda \alpha!}{\lambda!(\alpha - \lambda)!}\sqrt{\frac{(2\lambda)!(2\alpha - 2\lambda + 1)!}{(2\alpha + 1)!}} =$$

$$= \frac{(-1)^{(\alpha-\ell)}\alpha!}{(\alpha - \ell)!\ell!}\sqrt{\frac{(2\alpha - 2\ell)!(2\ell + 1)!}{(2\alpha + 1)!}}, \qquad (4.2.20)$$

only one term remains from the inner sum of Eq. (4.2.18):

$$\sum_{\lambda=0}^\infty \left(C_{\alpha 0 \ \lambda 0}^{\ell \ 0}\right)^2 = \left(C_{\alpha 0 (A-B) 0}^{\ell 0}\right)^2 = \left(\frac{C_A^B}{\sqrt{C_{2A}^{2B}}}\right)^2, \qquad (4.2.21)$$

---

[6]in [87]: Eq.8.5.2.(33)

[7]in [87]: Eq.8.5.2.(34)

where C_n^k are binomial coefficients, $A = \max(\ell, \alpha)$, $B = \min(\ell, \alpha)$. Finally, the diagonal part of the HF potential becomes:

$$V_\ell^H(r, \ r) - V_\ell^F(r, \ r) = \sum_{\varepsilon \ \alpha} \frac{2\alpha + 1}{2\ell + 1} \ \frac{u_{\varepsilon\alpha}^2(r)}{r} \left(1 - \frac{\left(C_A^B\right)^2}{C_{2A}^{2B}} \right). \qquad (4.2.22)$$

4.3 Self-consistency cycle

Now we can, of course, solve the system (4.1.4) in the way, equivalent to the conventional HF solution: since the functions α_{ℓ_i} and f_{ℓ_i} completely and uniquely restore the wave function, the usual self-consistency procedure (SCP) can be applied. Namely, at the first run of the integration procedure all n pairs of equations (4.1.4) are solved for $V^{ext}(r)$. Then the obtained wave functions, constructed from $\alpha_{\ell_i}, f_{\ell_i}$, are used to build the first iteration of the HF potential, in which the new set of eigenenergies and the new set of functions $\alpha_{\ell_i}, f_{\ell_i}$ can be calculated, and so on. In other words, the cycles of the SCP are *external* with respect to the integration of the system (4.1.4).

In case the energy spectrum of the HF problem is already known, it is possible to suggest a faster calculation scheme. Its main feature consists of performing the SCP *inside* the integration of the system (4.1.4). For this we use the property of the equation for the SA function, that the nonlocality has to be integrated on the finite (rather than infinite, as in conventional HF techniques) interval $[0 \dots r]$. For the calculation of the derivative $\dot{f}(R)$ at a certain point R it is not required to know the values of the function $f(r)$ at $r > R$. In other words, the value of the SA function $f(R) = \int_0^R \dot{f}(r) dr$ at a certain point R is not affected by the potential $V(r, r')$ (and, obviously, by any changes of $V(r, r')$ due to SCP) at $r, r' > R$. Basing on this property, it is possible to perform SCP inside any interval $[0 \dots R]$, in particular,

within the first mesh interval $[r_0, r_1]$.

The numerical algorithm is the following. For the arbitrary mesh $(r_0 = 0, r_1, \dots r_k, \dots r_{N-1}, r_N = \infty)$ one calculates the first pair $f_1(r_1), \alpha_1(r_1)$ in the absence of the inter-electron interaction. Then one starts the SCP: using $V(r, r')|_{r, r' \leq r_1}$, produced by the first pair, we calculate the functions of the second electron $f_2(r_1), \alpha_2(r_1)$ at the same mesh point r_1. Using $V(r, r')|_{r, r' \leq r_1}$, produced now by the first and the second pairs, one calculates $f_3(r_1), \alpha_3(r_1)$ and so on. After the calculation of the last pair $f_n(r_1), \alpha_n(r_1)$ we return to the first pair and repeat the process until convergency. After that we come to the the next point of the mesh and repeat previous manipulations. The physical sense of the found solution is the following. Consider the potential for i-th electron, created by all the other electrons in the k-th mesh point. Consider the self-consistent set $A_k = \{f_j(r_m), \alpha_j(r_m)\}_{j \neq i}^{m=0..k}$. Wave functions, constructed from it, coincide with the true single-electron HF wave functions up to the point r_k. The nonlocal potential $V_i^{(k)}(r, r')$, produced by A_k, coincides with the exact HF potential cut-off at $r = r' = r_k$ and is not defined at larger distances. Going to the $(k+1)$-th mesh point, one needs to calculate $f_j(r)$ and $\alpha_j(r)$ only in this very point, because, as mentioned above, their values in the previous k points have been already calculated and will be not affected by the potential in the last, $(k+1)$-th, point. Finally, the potential produced by the set A_n, given on the whole mesh, is nothing but the true HF potential.

Fast convergence of the SCP is due to the following reasons:

i) the SCP starts almost from the very beginning of the integration, the inter-electron potential is added already for the wave-amplitude and scattering-amplitude functions of the second electron of the system. Even in the first cycle of the SCP,

as the number i of the pair $(f_{\ell_i}, \alpha_{\ell_i})$ in (4.1.4) grows, the accounted inter-electron potential becomes more and more close to exact;

ii) moving along the mesh does not change the values of the functions, calculated in the previous points. The inter-electron potential, used for the calculations at each mesh point, differs from the exact potential only in the last mesh point.

Although it is hard to expect that the eigenenergies of the HF problem may be known in advance, we would like to emphasize that the proposed idea of the self-consistent solution of the systems of differential equations *within* the integration mesh deserves further consideration for different physical problems (especially those with rapidly changing or fast oscillating solutions).

As a numerical example, consider the case of the nonlocal mean-field potential for the case of negative hydrogen ion, arising on the first step of the Hartree-Fock SCP. Suppose one electron occupying 1s-state and the other one – some another s-state, i.e. hydrogen ion is excited (this choice is made solely for the simplicity of the potentials). The Slater expansion of the interelectron interaction reads

$\frac{1}{|\mathbf{r}-\mathbf{r}'|} = \frac{1}{r} \sum_{\lambda=0}^{\infty} (\frac{r'}{r})^{\lambda} P_{\lambda}(\cos(\widehat{\mathbf{r}\mathbf{r}'}))$. Together with the nonlocal density of 1s-electron $\rho(r, r') = (e^{-2r'} - e^{-r}e^{-r'})/4\pi$ and with the selection rule

$\int_{-1}^{1} P_{\ell}(\cos(\mathbf{r}\widehat{}\mathbf{r}'))P_{\lambda}(\cos(\mathbf{r}\widehat{}\mathbf{r}'))d(\mathbf{r}\widehat{}\mathbf{r}') = \delta_{\ell\lambda}$, which leaves only one term in the Slater expansion, it gives the nonlocal potential for the *ns*-electron $W = \frac{1}{r}\left[e^{-2r'} - e^{-r}e^{-r'}\right]$. In Fig. 4.1 we explore the role of the nonlocality as introduced by the potentials $V_F = -e^{-r}e^{-r'}/4\pi$ and $V_H = e^{-2r'}/4\pi$ corresponding to the Fock and Hartree terms respectively. Function $\gamma_0(r)$ for the bare Coulomb electron-ion interaction (C), Coulomb plus Fock-term (CF), Coulomb plus Hartree-term (CH) and all three terms together (CHF) is depicted. The inset shows the corresponding cut-off distances, at which

these potentials acquire the 8-th s-state $(\gamma_0(r)=\frac{15}{2}\pi)$. The smaller is this distance the larger is the strength of the potential. The strongest is the potential V_{CF}, which contains two attractive terms, then comes the bare Coulomb potential. Slightly more shallow is the total potential V_{CHF}, containing two attractive and one repulsive term. This is reflected, for example, in the extrusion of the highest Coulomb bound states in the continuum when the interelectron interaction is switched on. The most weak is V_{CH}, lacking the attractive exchange term.
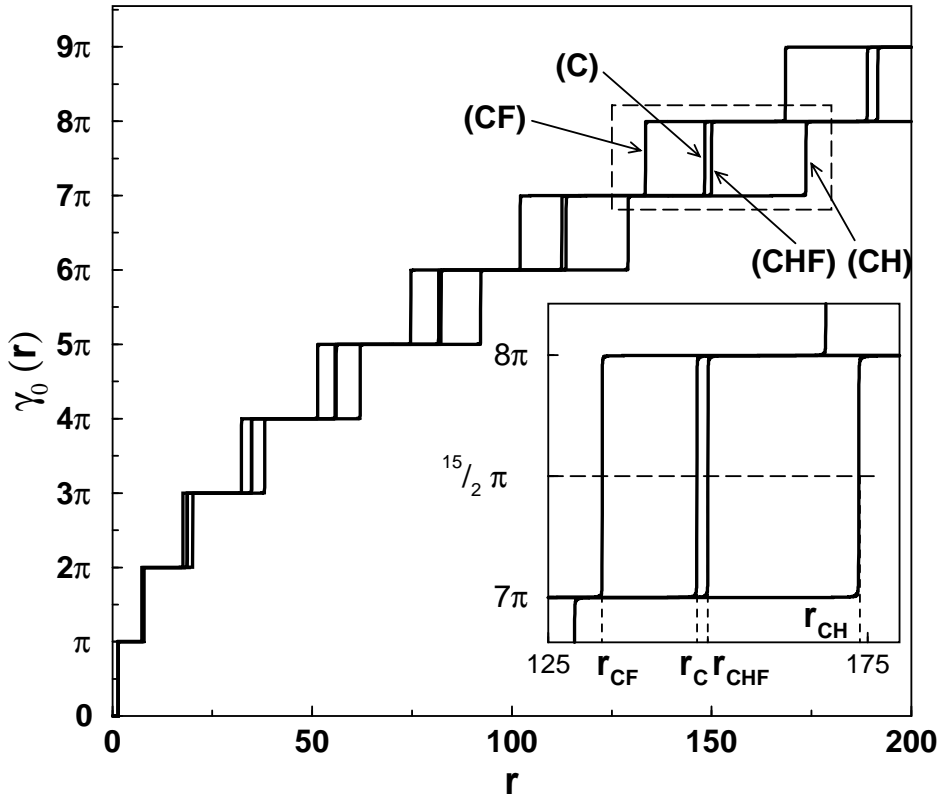

Figure 4.1: Function $\gamma_0(r)$ for the local $V_C = -1/r$, and for the different nonlocal potentials V_{CF}, V_{CH}, V_{CHF} (for the explanation see text). In all cases the energy is the same: $E = -0.5 \times 10^{-10}$. Inset: the behavior of $\gamma_0(r)$ in the vicinity of $\gamma_0(r) = \frac{15}{2}\pi$.

Chapter 5

Random phase approximation as a tool for correlation studies

This chapter describes the electronic correlation effects in terms of the first-order response of the system to the external perturbation. The relation between the static and the dynamic screening in the Thomas-Fermi model and in the Random Phase approximation with Exchange (RPAE) is discussed in Sec. 5.1. Sec. 5.2 contains the derivation and the explanation of the physical essence of the RPAE equations.

5.1 Static and dynamic screening

The primary source of knowledge on the structure and the dynamics of electronic systems is provided by their characteristic response to external perturbations. For systems with a large number of active electrons, such as clusters and surfaces, the collective response is determined basically by the cooperative behavior of the system's constituents, e.g. the delocalized electrons in a metallic surface shield, by an organized

rearrangement, an external electric field which might be induced by an approaching test charge. These correlated fluctuations of the electronic density, i.e. the excitation and de-excitation of electron-hole pairs, can be described by the so-called polarization operator Π (or the particle-hole propagator) [32]. The charge density fluctuations of the medium modify the properties of the electron-electron interaction U. The way how the modified potential U_{eff} emerges from the naked interaction U is determined by Π through the integral equation [32]

$$U_{eff} = U + U\Pi U_{eff}. \qquad (5.1.1)$$

This relation can be formally written as

$$U_{eff} = \kappa U, \qquad (5.1.2)$$

where $\kappa := 1/(1 - U\Pi)$, referred to as the inverse dielectric function [32], plays a central role in a variety of phenomena. To name one, the frequency (ω) and wave vector ($\mathbf{p}$) dependent electrical conductivity $\sigma(\mathbf{p},\omega)$ of a plasma is obtained from $\kappa(\mathbf{p},\omega)$ as $\sigma(\mathbf{p},\omega) = i\omega(1 - \kappa)$. This is just one of numerous examples for the fundamental interest in the study of the dynamical screening in electronic systems.

The determination of the renormalized interaction U_{eff} and of the dielectric function κ entails the knowledge of Π. In essence, Π is a two-point Green function that describes the particle-hole excitations. Its lowest order approximation Π_0 is provided by the so-called random phase approximation with exchange (RPAE) [32], diagrammatically represented in Fig. 5.1. For a homogeneous system and in the long wave-length limit ($\lambda \gg \lambda_F$, where λ_F is the Fermi wave length) one obtains $\Pi_0 \approx -2N(\mu)$. Here $N(\mu)$ is the density of states at the Fermi level μ. Hence, for $\lambda \gg \lambda_F$, the screened potential of the bare electron-electron interaction $U(\mathbf{q}) = 4\pi/q^2$ is readily derived
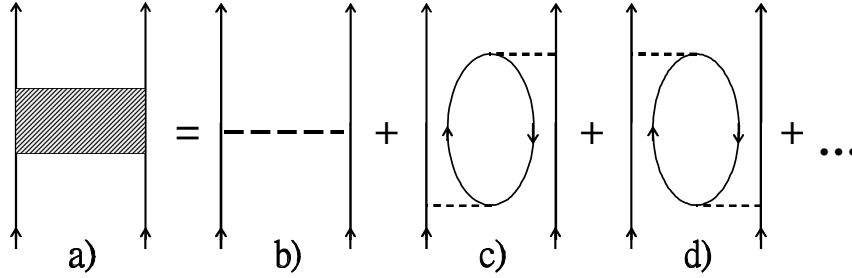
Figure 5.1: Diagrammatic description of relaxation of electron-electron interaction through screening: a) screened interaction; b) bare interaction; c) and d) lowest order dynamic screening corrections via particle-hole excitations.

as $U_{TF} = 4\pi/[q^2 + 8\pi N(\mu)]$. In configuration space we recover thus the well-known Thomas-Fermi potential $U_{TF} = e^{-r/r_0}/r$ $(r_0 = 1/\sqrt{8\pi N(\mu)})$. This form of the interaction gives a first hint on the nature of electronic collisions in extended many-particle systems: In an isolated scattering of two charged particles, events with a small momentum transfer q (far collisions) are predominant, for the naked potential behaves as $U \propto 1/q^2$. In contrast, these events are suppressed in the presence of a polarizable medium due to the finite range of the renormalized scattering potential U_{eff} which dictates that scattering can occur only at distances close enough such that the medium is not able to screen the external field $(\lim_{q \ll 1} U_{TF} \propto 1/[8\pi N(\mu)] = constant)$. Hence, we conclude that the scattering probability as a function of the impact parameter saturates at a distance d determined by the extent r_0 of the scattering region $(\lim_{r_0 \to \infty} d \to \infty)$. It is not clear from the outset that these calculations are also valid for finite size systems, such as metal clusters, for the eigenstates of these systems are not simply plane waves, and the properties of Π are still to be clarified.

5.2   RPAE matrix elements for finite systems

In this section we give the derivation of the expression for the RPAE matrix element [4] for the ionization of a system by an external perturbation, in particular, by a charged particle. Let $\widehat{H_0}$ be the Hamiltonian of a cluster. Under the action of an external field $\delta U(\mathbf{r}, t)$ the self-consistent cluster potential is changed and the Hamiltonian becomes: $\widehat{H}(\mathbf{r}, t) = \widehat{H_0}(\mathbf{r}) + \delta U(\mathbf{r}, t)$. Then, the ionization amplitude is given as a sum of two terms: first term corresponds to the removal of the electron due to the *direct* interaction with the external field, second one arises from the change of the cluster potential.

The total wave function is described as an antisymmetrized product of single-electron wave functions: $\Psi(\mathbf{r}_1, \mathbf{r}_2 \ldots \mathbf{r}_n, t) = e^{-iE_0 t} \det \|\psi_i(\mathbf{r}_j, t)\|$, where

$$E_0 = \sum_i \left\langle \phi_i \left| -\frac{\nabla_i}{2} - V^{ion} \right| \phi_i \right\rangle + \frac{1}{2} \sum_{i,k} \left\langle \phi_i \phi_k \left| u \right| \phi_i \phi_k - \phi_k \phi_i \right\rangle \tag{5.2.1}$$

is the Hartree-Fock ground state energy of the system and $u \equiv \frac{1}{|\mathbf{r}_i - \mathbf{r}_k|}$ is the bare Coulomb inter-electron interaction. Time-dependent single-electron wave functions $\psi_i(\mathbf{r}, t)$ can be expanded over the set of time-independent Hartree-Fock solutions $\phi(\mathbf{r})$:

$$\psi_i(\mathbf{r}, t) = A_i \left[\phi_i(\mathbf{r}) + \sum_m C_{mi}(t) \phi_m(\mathbf{r}) \right]. \tag{5.2.2}$$

Here indices m and i label the states above and below the Fermi level, A is a normalization coefficient, $C_{mi}(t)$ is the probability amplitude for the creation of the m-i electron-hole pair. The sum describes an admixture of the excited states m to the initial state i and implies a summation over unoccupied discrete levels and an integration over continuum.

Coefficients $C_{mi}(t)$ can be calculated by the solution of the Schrödinger equation for the total wave function:

$$\left\langle \Psi(\mathbf{r}_1, \mathbf{r}_2 \ldots \mathbf{r}_n, t) \middle| \widehat{H} - i\frac{\partial}{\partial t} \middle| \Psi(\mathbf{r}_1, \mathbf{r}_2 \ldots \mathbf{r}_n, t) \right\rangle = 0. \tag{5.2.3}$$

In the presence of the external field $C_{mi}(t) \neq 0$. Expanding Eq. 5.2.3 over these coefficients and taking into account the first non-vanishing terms, one gets

$$i\sum_{i \leq \varepsilon_F < m} C^*_{mi}(t)\frac{\partial}{\partial t}C_{mi}(t) = \sum_{i \leq \varepsilon_F < m} \left\{ (\varepsilon_m - \varepsilon_i) |C_{mi}(t)|^2 + C_{mi}(t) \left\langle i \middle| \delta U \middle| m \right\rangle + C^*_{mi}(t) \left\langle m \middle| \delta U \middle| i \right\rangle + \right.$$

$$\left. + \sum_{j \leq \varepsilon_F < k} \left[\frac{1}{2}C^*_{mi}(t)C^*_{kj}(t) \left\langle mk \middle| u \middle| ij \right\rangle + \frac{1}{2}C_{mi}(t)C_{kj}(t) \left\langle ij \middle| u \middle| mk \right\rangle + C^*_{mi}(t)C_{kj}(t) \left\langle mi \middle| u \middle| kj \right\rangle \right] \right\}.$$

Here $\left| \alpha \right\rangle \equiv \left| \phi_\alpha \right\rangle$.

Terms linear in $C_{mi}(t)$, excluding an external time-dependent field δU, disappear as a solution of the Hartree-Fock equation:

$$\left\langle m \middle| -\frac{\nabla}{2} - V_{ions} \middle| i \right\rangle + \sum_{j \leq \varepsilon_F} \left\langle mj \middle| u \middle| ij \right\rangle = 0. \tag{5.2.4}$$

Variation over $C^*_{mi}(t)$ gives

$$i\frac{\partial}{\partial t} C_{mi}(t) = (\varepsilon_m - \varepsilon_i) C_{mi}(t) + \left\langle m \middle| \delta U \middle| i \right\rangle +$$

$$+ \sum_{j \leq \varepsilon_F < k} \left[C^*_{kj}(t) \left\langle mk \middle| u \middle| ij \right\rangle + C_{kj}(t) \left\langle mj \middle| u \middle| ik \right\rangle \right]. \tag{5.2.5}$$

We search for the solution of this system in the form: $C_{mi}(t) = X_{mi}e^{-i\varepsilon_0 t} + Y^*_{mi}e^{i\varepsilon_0 t}$ with ε_0 being the energy transferred to the system. Finally, the system of coupled equations for these coefficients reads:

$$(\varepsilon_m - \varepsilon_i - \varepsilon_0) X_{mi} + \left\langle m \middle| \delta U \middle| i \right\rangle + \sum_{j \leq \varepsilon_F < k} \left[\left\langle mj \middle| u \middle| ki \right\rangle X_{kj} + \left\langle mk \middle| u \middle| ji \right\rangle Y_{kj} \right], \tag{5.2.6}$$

$$(\varepsilon_m - \varepsilon_i + \varepsilon_0) Y_{mi} + \left\langle i \left| \delta U \right| m \right\rangle + \sum_{j \le \varepsilon_F < k} \left[\left\langle ij \left| u \right| km \right\rangle X_{kj} + \left\langle ik \left| u \right| jm \right\rangle Y_{kj} \right] . \quad (5.2.7)$$

If both the time-independent part of the field δU and the inter-electron interaction u are absent, X and Y, which become independent solutions, describe the electron excitation (de-excitation) from i to m, respectively. Representing the unknown coefficients X_{mi} and Y_{mi} through the matrix elements of the effective field operator δU_{eff}

$$-(\varepsilon_m - \varepsilon_i - \varepsilon_0) X_{mi} \equiv \left\langle m \left| \delta U_{eff} \right| i \right\rangle \text{ and } -(\varepsilon_m - \varepsilon_i + \varepsilon_0) Y_{mi} \equiv \left\langle i \left| \delta U_{eff} \right| m \right\rangle,$$

we can write down the required equation for the ionization amplitude

$$\left\langle m \left| \delta U_{eff} \right| i \right\rangle = \left\langle m \left| \delta U \right| i \right\rangle +$$

$$+ \sum_{j \le \varepsilon_F < k} \left[\frac{\left\langle k \left| \delta U_{eff} \right| j \right\rangle \left\langle mj \left| u \right| ki \right\rangle}{\varepsilon_0 - \varepsilon_k + \varepsilon_j + i\nu} - \frac{\left\langle j \left| \delta U_{eff} \right| k \right\rangle \left\langle mk \left| u \right| ji \right\rangle}{\varepsilon_0 + \varepsilon_k - \varepsilon_j - i\nu} \right] . \quad (5.2.8)$$

Eq. (5.2.8) is the main RPAE equation for the transition amplitude under the action of the *effective* external field. It can be viewed as a generalization of the HF equations, allowing to take into account the response of the cluster electrons to the bare external perturbation. The first term in the right-hand side of (5.2.8) describes the *direct* excitation of the electron by the bare external field. The second and the third terms, referred to as *correlation* terms, describe more complex transitions with the participation of another electrons of the system, in which the ionization of the electron is mediated by the creation/annihilation of all possible electron-hole pairs. In this way, the correlations are included as a modification of the external perturbation, acting on the ionized electron, by the mobile electronic cloud of the system and enter the matrix elements of the form $\left\langle k \left| \delta U_{eff} \right| j \right\rangle$. Along with this, the creation of the electron-hole pairs occurs under the action of the naked electron-electron interaction: $\left\langle mj \left| u \right| ki \right\rangle$. Due to the long-range character of u, there is a certain difficulty in the calculation of the numerous Coulomb matrix elements of these transitions, because

in Eq. (5.2.8) one should sum over all possible electronic excitations. There is another useful form of this equation, where the renormalization of the external field is expressed in terms of a renormalized two-particle interaction in the system

$$
\left\langle m \left| \delta U_{eff} \right| i \right\rangle = \left\langle m \left| \delta U \right| i \right\rangle +
$$
$$
+ \sum_{j \leq \varepsilon_F < k} \left[\frac{\left\langle k \left| \delta U \right| j \right\rangle \left\langle mj \left| u_{eff} \right| ki \right\rangle}{\varepsilon_0 - \varepsilon_k + \varepsilon_j + i\nu} - \frac{\left\langle j \left| \delta U \right| k \right\rangle \left\langle mk \left| u_{eff} \right| ji \right\rangle}{\varepsilon_0 + \varepsilon_k - \varepsilon_j - i\nu} \right]. \quad (5.2.9)
$$

Here U is the bare external field and u_{eff} is the effective electron-electron interaction. Its matrix elements can be found from

$$
\left\langle mj \left| u_{eff} \right| ki \right\rangle = \left\langle mj \left| u \right| ki \right\rangle +
$$
$$
+ \sum_{p \leq \varepsilon_F < q} \left[\frac{\left\langle qj \left| u \right| kp \right\rangle \left\langle mp \left| u_{eff} \right| qi \right\rangle}{\varepsilon_0 - \varepsilon_p + \varepsilon_q + i\nu} - \frac{\left\langle pj \left| u \right| kq \right\rangle \left\langle mq \left| u_{eff} \right| pi \right\rangle}{\varepsilon_0 + \varepsilon_p - \varepsilon_q - i\nu} \right]. \quad (5.2.10)
$$

Chapter 6

Electron and proton impact ionization of C_{60} and metal clusters

In the first part of this chapter we describe model potentials for the systems under study and their energy structure. In Sec. 6.2 the fluctuations in the electronic charge density of the clusters in response to an approaching electron are investigated for the electron impact ionization of C_{60} and Li_n clusters. The suppression of the single ionization channel is revealed by RPAE calculations and analyzed in the Thomas-Fermi model of screening. The interplay between finite size and nonlocal screening effects is studied by tracing the changes in the ionization cross sections for Li clusters with an increasing cluster radius. In Sec. 6.7 the role of exchange correlation is revealed by comparing the cross sections for proton and electron impact collisions.

6.1   Confining potentials

Due to the large number of electrons in the fullerene molecule, *ab initio* calculations even of the single-particle wave functions and of the energy levels are practically impossible. They are performed, as a rule, within the frame of some phenomenological approach in which a model potential of fullerene shell is used, see e.g. [3, 15, 57, 89]. Naturally, preference should be given to a model that has the minimal set of fitting parameters. We employ the model having three experimentally observed parameters, namely, radius and thickness of the fullerene shell and the affinity energy of the electron to the singly charged fullerene.

The potential of C_{60}, formed by carbon ions and localized core electrons, is re-placed by a shifted potential well: $V(r) = V_0$ within the interval $R - \Delta R < r < R + \Delta R$, and $V = 0$ elsewhere. Here $R \approx 6.65\ a_0$ is the radius of the fullerene [85], the thickness of the shell is $2\Delta R \approx 2a_0$, a_0 being the Bohr radius. The depth of the well is chosen such that to reproduce the experimental value of first ionization potential of C_{60}, which is 7.1 eV [52, 75, 80] and to encompass 240 valence electrons. Despite the simple potential structure this model is a good tool for analytical esti-mations providing clear insight into phenomenology of the object and the processes under consideration. Moreover, as it will be shown in Sec. 6.2, the simple many-body improvement of this model done by the Hartree-Fock description of the eigenstates of the target together with the Thomas-Fermi approach for the interaction with the probe particle yields encouraging results when compared with available experimental data for electron impact ionization of C_{60} clusters.

Due to the shift R of the potential well from the origin (the center of spherical symmetry) the energy structure of the levels has an interesting form. An example of

this energy structure for the shifted square well is shown in Fig. 6.1. It consists of several branches, each branch is characterized by the fixed number of nodes of the corresponding wave function. Namely, the wave functions of the zero-branch (black curve in Fig. 6.1) have no nodes, states on the next branch (blue curve) have one node, etc. The levels belonging to the different branches are well separated in
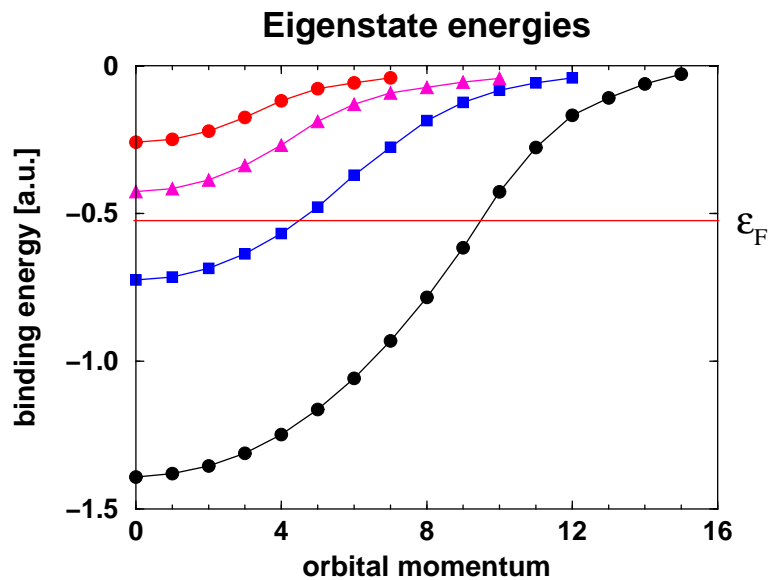

Figure 6.1: Example of the energy structure of the shifted rectangular well as a function of orbital momentum. Each branch of eigenstates is characterized by the fixed number of nodes n_r of the corresponding wave function (black curve: $n_r = 0$, blue curve: $n_r = 1$, etc.)

energy, at least for the small orbital momenta. The energy of the level on the same branch grows with the orbital number. With increase of the shell radius R (with the constant potential width $2\Delta R$) the energy structure changes: the larger is the shift the more flat are the branches. In the limit, when the shift goes to infinity all branches transform to lines parallel to x-axis because all levels with the same number of nodes
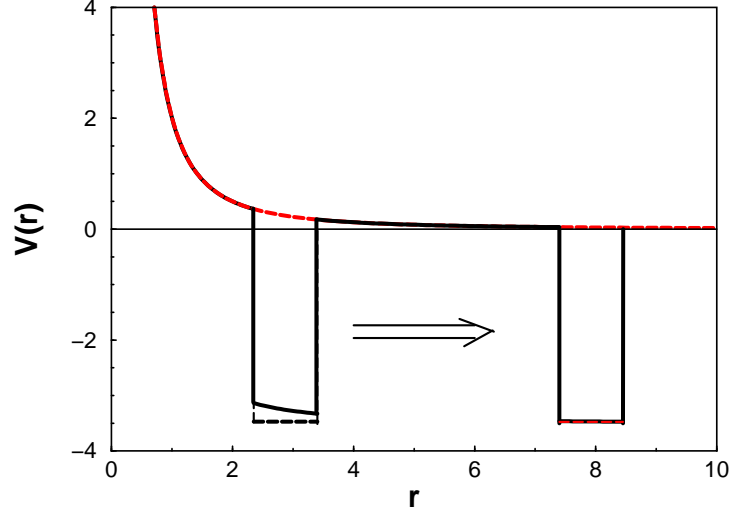
Figure 6.2: Effect of the centrifugal term on the shell potential for different shell radii. In the large R limit the centrifugal term gives negligible contribution.

become degenerate in energy $E = E_{\ell=0}$. This behavior is clear from the Shrödinger equation. At large distances and large R the centrifugal term becomes negligible with respect to V_0 (see Fig. 6.2) and the equation transforms to the one-dimensional equation for the finite square well:

$$-\frac{d^2\psi_\ell(r)}{dr^2} + \left(\frac{\ell(\ell+1)}{r^2} - V_0(r \in [R \pm \Delta R])\right)\psi_\ell(r) = E\psi_\ell(r) \quad \longrightarrow_{R\to\infty}$$

$$\longrightarrow \quad -\frac{d^2\psi_\ell(r)}{dr^2} - V_0(r \in [R \pm \Delta R])\psi_\ell(r) = E\psi_\ell(r). \tag{6.1.1}$$

The quantum states of the clusters are constructed within the HF approximation. Hartree-Fock model is principally the best out of single-particle theories in a sense that it is able to incorporate part of electron-electron interactions and exchange. In this model each electron moves in a self-consistent averaged electric field of all the other electrons of the system, obeying Pauli principle. The one-electron potential then represents a sum of the ionic background and self-consistent electronic density

of the valence electrons. The bound state wave functions are calculated in the frame of the nonlocal variable phase approach (Sec. 3.4). The eigenenergies are determined by finding the poles of the partial scattering amplitude on the imaginary semi-axis of the wavevector $k = i\kappa$, $\kappa \in \Re$. (c.f. Eq. 3.4.14).

In total, there are 16 occupied orbitals in C_{60}. The lowest 10 of them are such that their wave functions with the orbital momenta $0 \leq \ell \leq 9$ have no nodes. Then 4 orbitals with $0 \leq \ell \leq 3$ have one node and two highest occupied orbitals with $0 \leq \ell \leq 1$ have two nodes. Each orbital is $2 \cdot (2\ell + 1)$ degenerate. All shells are closed and the total number of the electrons is equal to 240. Lithium clusters with different
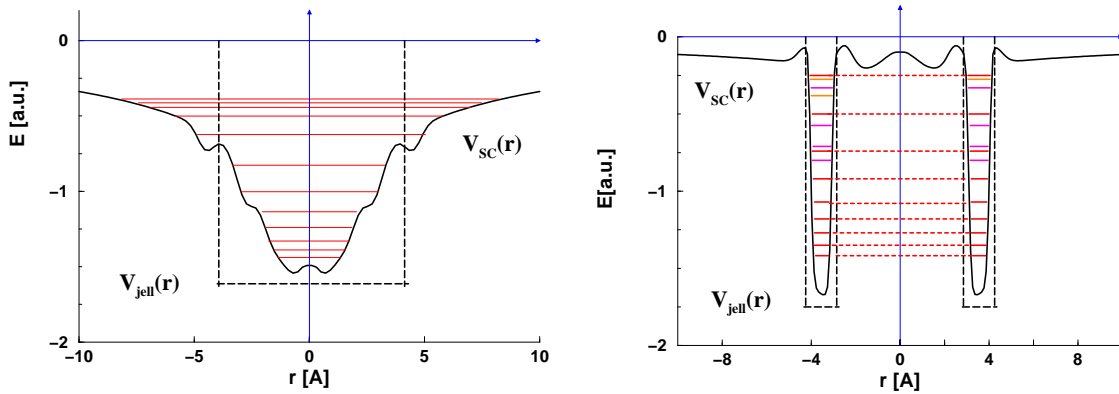

Figure 6.3: The local part of one-electron HF potential of a) Li_{44} and b) C_{60}, calculated in the spherical jellium and jellium shell models.

number of atoms were chosen as an example of typical metallic particles. Basing on the same jellium potential model and within the VPA we performed the Hartree-Fock calculations of the eigenstates of Li_4, Li_8, Li_{18}, and Li_{44}. The parameters of the rectangular well were again taken such that to reproduce the first ionization potential [29] and to contain all delocalized electrons.

The self-consistent electronic density smoothes the sharp potential edges and introduces slight oscillations in the potential profile. The local parts of the self-consistent nonlocal one-electron potentials for the ground states of C_{60} and Li_{44} clusters are shown in Fig. 6.3

6.2 Manifestation of charge density fluctuations in metal clusters: suppression of the ionization channel

In this section we consider the influence of nonlocal screening on the single ionization of fullerene clusters by electron impact and show that the fluctuations of the electronic charge density of metallic clusters in response to an approaching electron suppress the single ionization channel. The present numerical results performed in the random phase approximation and analyzed by means of the Thomas-Fermi model of screening explain the behavior of the measured total ionization cross section for C_{60}. In addition, we investigate the interplay between quantum size and non local screening effects by tracing the changes in the ionization cross sections for Li clusters with an increasing cluster radius.

The ideas sketched in the previous chapter are the key to resolve a yet open question of how metal clusters ionize in response to an external perturbation induced by an approaching electron. In the experiments, which have been performed using free C_{60} clusters, one measures the absolute total ionization cross sections $W(\epsilon_0)$, i.e. the yield for the C_{60}^+ production, as function of the energy (ϵ_0) of an incoming

electron [58, 34, 81]. These measurements confirmed repeatedly that the cross section $W(\epsilon_0)$ possesses a plateau shape: Near the ionization threshold it rises strongly with increasing ϵ_0 and then falls off slowly at higher energies. This saturation effect is markedly different from what is known for atomic targets where $W(\epsilon_0)$ shows a pronounced peak at low ϵ_0 (c.f. Fig. 6.4a).

Theoretical attempts to explain the behavior of $W(\epsilon_0)$ for C_{60} are scares. For the energy region $\epsilon_0 < 100\, eV$ only semi empirical models exist [27, 81] whereas for $\epsilon_0 > 100\, eV$ a quantum scattering approach has been proposed in Refs. [46, 45]. All of these previous theories [81, 27, 46, 45] were unable to explain the energy dependence of $W(\epsilon_0)$, basically because the problem has been approached from an atomic scattering point of view without account for the influence of the fluctuating electron density on the scattering process which is of a key importance at low energies ($\epsilon_0 < 1000\, eV$), as shown here in details: The central quantity that determines $W(\epsilon_0)$ is the transition matrix element $T(\mathbf{k}_0, \phi_\nu; \mathbf{k}_1, \mathbf{k}_2)$. This matrix element is a measure for the probability that an incoming electron with momentum $\mathbf{k}_0$ ionizes a valence electron bound to the state ϕ_ν of the cluster with a binding energy ϵ_ν, where ν stands for a collective set of quantum numbers that quantify uniquely the electronic structure of the cluster. The emitted and the scattered electrons' states are labelled by the momenta $\mathbf{k}_1$ and $\mathbf{k}_2$. As outlined above the renormalized electron-electron interaction U_{eff} is determined by an integral equation with a kernel describing the particle-hole (de)excitation. Therefore, the evaluation of the T matrix entails a self-consistent solution of an integral equation. In the random-phase approximation with exchange [32] and within the *post* formulation [84] the T matrix has the form $T_{RPAE} = \left\langle \mathbf{k}_1 \mathbf{k}_2 \right| U_{eff} \left| \phi_\nu \mathbf{k_0} \right\rangle$ where (c.f. Eq. 5.2.9)

$$\left\langle \mathbf{k_1 k_2} \right| U_{eff} \left| \phi_\nu \mathbf{k_0} \right\rangle = \left\langle \mathbf{k_1 k_2} \right| U \left| \phi_\nu \mathbf{k_0} \right\rangle +$$

$$+ \sum_{\varepsilon_p \leq \mu < \varepsilon_h} \left(\frac{\left\langle \varphi_p \mathbf{k_2} \right| U_{eff} \left| \phi_\nu \varphi_h \right\rangle \left\langle \varphi_h \mathbf{k_1} \right| U \left| \mathbf{k_0} \varphi_p \right\rangle}{\epsilon_0 - (\varepsilon_p - \varepsilon_h - i\delta)} - \right.$$

$$\left. - \frac{\left\langle \varphi_h \mathbf{k_2} \right| U_{eff} \left| \phi_\nu \varphi_p \right\rangle \left\langle \varphi_p \mathbf{k_1} \right| U \left| \mathbf{k_0} \varphi_h \right\rangle}{\epsilon_0 + (\varepsilon_p - \varepsilon_h - i\delta)} \right) . \quad (6.2.1)$$

The spin averaged cross section $W(\epsilon_0)$ is obtained from the weighted average of the singlet $\propto |T^{(S=0)}|^2$ (vanishing total spin ($S = 0$) of the electron pair) and the triplet $\propto |T^{(S=1)}|^2$ cross sections (we assume spin-flip processes to be irrelevant)

$$W(\epsilon_0) = \frac{(2\pi)^4}{k_0} \int d^3 \mathbf{k_1} d^3 \mathbf{k_2} \left\{ \sum_\nu \frac{1}{4} \left| T^{(S=0)}(\mathbf{k_0}, \phi_\nu; \mathbf{k_1}, \mathbf{k_2}) \right|^2 + \right.$$

$$\left. + \frac{3}{4} \left| T^{(S=1)}(\mathbf{k_0}, \phi_\nu; \mathbf{k_1}, \mathbf{k_2}) \right|^2 \right\} \delta \left(\epsilon_0 + \epsilon_\nu - (k_1^2/2 + k_2^2/2) \right). \quad (6.2.2)$$

In Eq. (6.2.1) φ_p and φ_h are respectively the intermediate particle's and hole's states with the energies ε_p, ε_h whereas δ is a small positive real number. The first line of Eq. (6.2.1) amounts to a neglect of the electron-hole (de)excitations, as done in Ref. [45]. If U_{TF} is employed as an effective potential only the first line of Eq. (6.2.1) has to be evaluated and we obtain the much simpler expression $T_{TF} = \left\langle \mathbf{k_1 k_2} \right| U_{TF} \left| \phi_\nu \mathbf{k_0} \right\rangle$ from which the cross section W_{TF} follows according to Eq. (6.2.2). In contrast, as evident from Eqs. (6.2.1, 6.2.2), the numerical evaluation of $W(\epsilon_0)$ within RPAE is a challenging task. To tackle this problem we proceeded as follows: The quantum states of the metal clusters are constructed within the Hartree-Fock approximation and within the spherical jellium model. Alternatively, one can employ a model cluster potential as derived from the density functional theory (DFT)

within the local density approximation [45]. As shown below the DFT potential leads basically to the same conclusions as the model potential outlined above.

As remarked in Refs. [45, 46], the relatively large size of the cluster leads to severe convergence problems in evaluating the transition matrix elements. To circumvent this situation we utilized the nonlocal variable phase approach [7, 21, 47] for the numerical calculation of the Hartree-Fock states. We find that this choice for the numerical realization renders a rapid and a reliable convergence of the self-consistent calculations. Upon the numerical summation over the states ϕ_ν in Eq. (6.2.2) we carry out the six-dimensional integral over the momenta $\mathbf{k}_1$ and $\mathbf{k}_2$ using a Monte-Carlo procedure. To get an insight into the effect of the screening we calculated $W_{TF}(\epsilon_0)$ for different values of the screening length r_0. As seen in Fig. 6.4(a), when approaching the unscreened limit ($r_0^{-1} = 0.01\,a.u.$), the calculated $W_{TF}(\epsilon_0)$ agree well both in shape and magnitude with the finding of Ref. [27] at lower energies. At higher energies, the present model and the DFT calculations [45, 46] yield basically the same results. To simulate experimentally this atomic case let us assume the C_{60} molecule to be simply an ensemble of 60 independent carbon atoms in which case the cross section for C_{60} is a factor 60 larger than $W(\epsilon_0)$ for atomic carbon [17]. The experimental cross sections we obtain by this procedure (Fig. 6.4(a)) agree very well with the shape of the calculated $W_{TF}(\epsilon_0)$ at low screening. On the other hand, all of the theoretical models shown in Fig. 6.4(a) are clearly at variance with the measured $W(\epsilon_0)$ for C_{60} (note the measured and the calculated cross sections are on an absolute scale). Fig. 6.4(b) sheds light on the underlying reasons for the shortcomings of the theories shown in Fig. 6.4(a): with increasing screening the region where scattering may take place shrinks. This results in a suppression of the ionization cross section
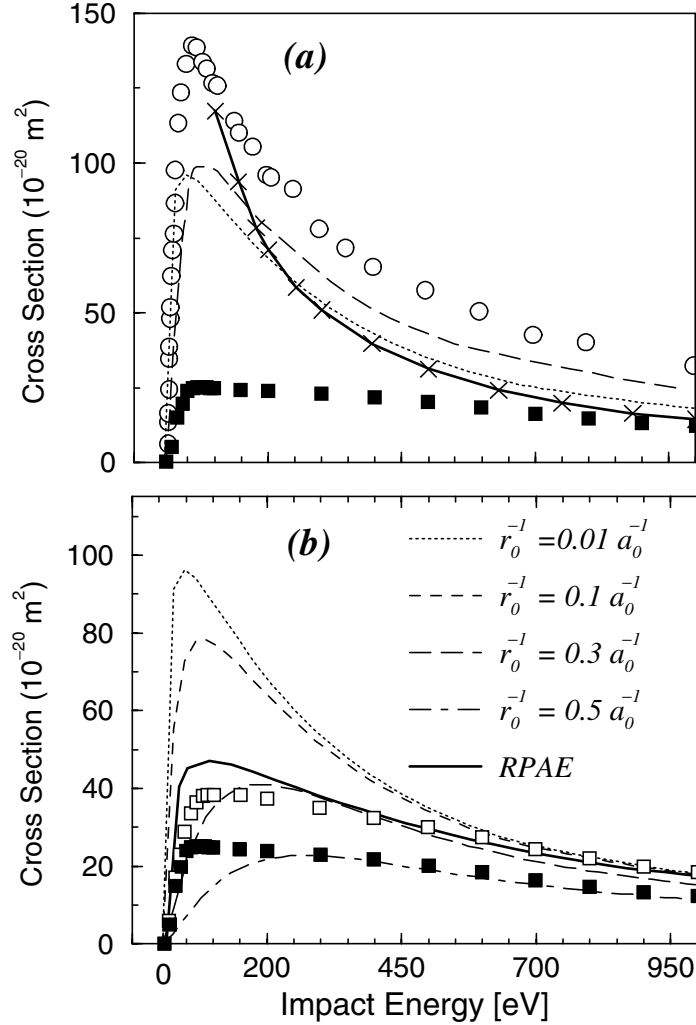
Figure 6.4: (a) The total ionization cross-section (Eq. 6.2.2) for the electron impact single ionization of C_{60} as function of projectile energy. The *absolute* experimental data (full squares) for the production of stable C_{60}^+ ions [58, 34] are shown along with the experimental electron-impact total ionization cross sections for atomic carbon (open circles) [17] multiplied by a factor of 60 (c.f. text). The solid line with crosses is the results of the DFT calculations [46] whereas the dashed line is due to the model of Ref. [27]. The dotted line indicates the present calculations with very small screening ($r_0^{-1} = 0.01 \, a.u.$). /newline (b) The RPAE results (solid line) are shown together with calculations employing the Thomas-Fermi model of screening with varying values of the screening length, as shown on the figure. Full squares as in (a) whereas the open squares are the *absolute* experimental total counting cross-section for the emission of one electron from the initially neutral cluster (c.f. text for details) [58, 34].

with increasing screening length, as evident from Fig. 6.4(b). This effect is not a simple scaling down of $W(\epsilon_0)$, but the shape is also affected. The peak of $W(\epsilon_0)$ is shifted to higher energies and $W(\epsilon_0)$ is generally flattened. In fact for extremely high screening the cross section is very small and shows basically very weak dependence on ϵ_0. This can be understood from the behavior of the form factor of the potential U_{TF} which for large screening is independent of ϵ_0, i.e. $U_{TF}(q) \propto r_0^2 = constant, \; \forall \; \epsilon_0$. This behavior and the rough positions of the peaks in $W(\epsilon_0)$ can be explained analytically if we write $T_{TF} = \int d^3\mathbf{p}_1 d^3\mathbf{p}_2 \left\langle \mathbf{k}_1\mathbf{k}_2 \left| U_{TF} \right| \mathbf{p}_1\mathbf{p}_2 \right\rangle B$, where $B = \langle \mathbf{p}_1\mathbf{p}_2 | \phi_\nu \mathbf{k}_0 \rangle$, and assume B to vary slowly with $\mathbf{p}_1, \mathbf{p}_2$ on the scale of the variation of the form factor of U_{TF} (see Fig. 6.5 for illustration). Another extreme limit that shows up in Fig. 6.4 (c.f. also Fig. 6.6) is that when ϵ_0 is very large the electronic density of the cluster can not react within the very short passage time of the electron through the interaction region and hence only small deviations between all the models are observed in the high energy regime.

The full numerical RPAE calculations for the cross section $W_{RPAE}(\epsilon_0)$ confirm the trends we pointed out by means of the locally screened potential U_{TF}. In fact by comparing the $W_{RPAE}(\epsilon_0)$ and $W_{TF}(\epsilon_0)$ one may deduce a rough estimate of the screening length which is of importance for the consideration of the relaxation time due to electron-electron collisions [28]. We obtain a qualitative agreement between $W_{RPAE}(\epsilon_0)$ and $W_{TF}(\epsilon_0)$ when $r_0^{-1} = 0.3 \, a.u.$ is used to evaluate $W_{TF}(\epsilon_0)$, however it should be stressed that we were not able to reproduce correctly the RPAE calculations by simply adjusting r_0, as can be concluded from Fig. 6.4(b).

For a comparison of $W_{RPAE}(\epsilon_0)$ with the experiments we recall the remarks of Ref. [27] that, experimentally the electron-impact on C_{60} may lead not only to the
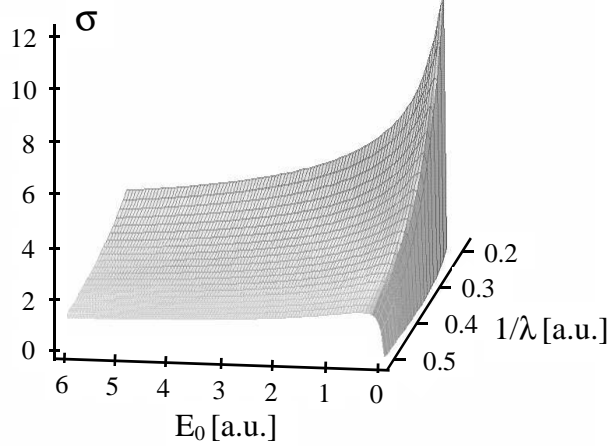
Figure 6.5: Schematic illustration of the variation of the electron-impact ionization cross section as a function of the impact energy E_0 and the screening length λ: $\sigma \sim \int d^3\mathbf{k}_1 d^3\mathbf{k}_2 |U_{eff}(q)|^2 \cdot |\widetilde{\Phi}(p)|^2 \sim \int d^3\mathbf{k}_1 d^3\mathbf{k}_2 \left|\frac{1}{q^2+1/\lambda^2}\right|^2 |\widetilde{\Phi}(p)|^2$, $\mathbf{p} = \mathbf{k}_0 - \mathbf{k}_1$, $\mathbf{q} = \mathbf{k}_0 - \mathbf{k}_1 - \mathbf{k}_2$.

formation of stable C_{60}^+ but also may produce unstable C_{60}^+ that within a certain lifetime, not resolved by the experiment, decay subsequently into various fragmentation channels. Therefore, we show in Fig. 6.4(b) the experimental total counting rates, i.e. the total electron-impact ionization cross sections for the emission of one electron from C_{60} along with the experimental total cross section for the ionization of C_{60} and for the formation of the stable C_{60}^+ ion. We regard the agreement between the parameter-free $W_{RPAE}(\epsilon_0)$ and the experimental results as satisfactory, in view of the fact that the RPAE is the first order approximation to the two-point particle-hole Green function. To study the interplay between quantum-size effects and the nonlocal screening as described by RPAE we calculated within the spherical jellium model the cross section $W_{RPAE}(\epsilon_0)$ for Li clusters with varying sizes. For a judicious conclusions
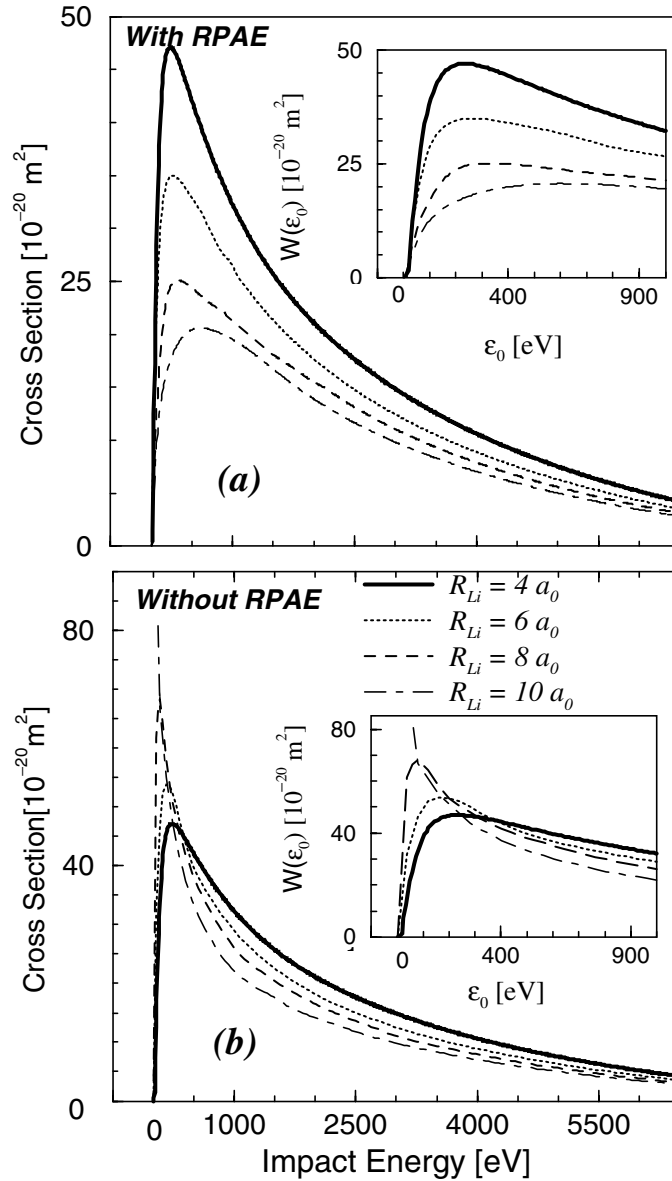
Figure 6.6: The total electron-impact cross section for the ionization of spherical Li clusters with varying radius size R_{Li}. (a) shows the RPAE calculations. (b) shows the results when the particle-hole (de)excitation is neglected (the first line of Eq. (6.2.1)). The insets in (a) and (b) highlight the low-energy region.

we normalized the cross sections to the number of electrons in the respective cluster. Figs. 6.6(a,b) reveals a striking influence of charge density fluctuation on $W(\epsilon_0)$ in particular at low energies: The RPAE model predicts a suppression of $W_{RPAE}(\epsilon_0)$ with an increasing cluster size due the increasing phase space for the particle-hole creation (c.f. inset of Fig. 6.6(a)). In contrast the neglect of charge density fluctuations results in increased peak values of $W(\epsilon_0)$ for larger clusters. Furthermore, according to the RPAE, the peak in $W(\epsilon_0)$ is considerably broadened and shifted towards higher energies when the cluster size is increased (for the cluster with a radius $R_{Li} = 4\,a_0$ the peak is at $\epsilon_0 \approx 200\,eV$ whereas this peak is shifted to $\epsilon_0 \approx 700\,eV$ for $R_{Li} = 10\,a_0$) (c.f. Fig. 6.6(a) and inset). As explained above, this is consistent with the behavior of $W(\epsilon_0)$ with increased screening length. In contrast, the neglect of the particle-hole (de)excitations leads to cross sections with the peak positions being shifted towards lower energies as the cluster size grows (c.f. Fig. 6.6(b) and inset). For small clusters or for $\epsilon_0 \gg 1$ there is hardly an influence of charge density fluctuations (c.f. heavy solid lines in Fig. 6.6(a,b)).

Summarizing the above results, we have seen how the particle-hole (de)excitations suppress and modify the ionization cross sections for the electron scattering from neutral metal clusters. The simple Thomas-Fermi (TF) model of screening provided a useful tool to obtain global views on the role of delocalization of the electrons. The more elaborate random phase approximation confirmed and specified more precisely the understanding gained from the TF model. We also envisaged the inter-relation between quantum-size and screening effects. From a formal point of view, we note that to treat scattering processes in isolated few charged particle systems, such as in atoms

or small molecules, one has to deal with the infinite-range tail of the Coulomb interaction that precludes the use of standard methods [84] and induces multiple scattering between the collision partners up to very large distances. In contrast, the presence of the screening in systems with a large number of delocalized active electrons renders possible the use of standard scattering theory but on the considerable expense of actually calculating the nonlocal screening properties of the medium, e.g. as described by the polarization propagator Π. The crossover between the two cases is marked by a breakdown of the RPAE for dilute systems, where other methods such as the ladder approximation become more appropriate. In any case one has to bear in mind that, both from a practical and a conceptual point of view, approximate methods that perform well for few particle scattering may not be suitable for the treatment of delocalized many-particle systems (and vice versa).

6.3 Ionization by proton impact: estimation of exchange effects

With the use of particles and antiparticles as projectiles in collision experiments, many effects related to the projectile charge and mass have been identified, and a detailed picture of phenomena influencing single and multiple ionization of atoms have been obtained [50, 77]. Complete set of data for ionization of the system by e^+, e^-, p^+, p^- allows to trace the role of polarization and exchange effects. At high impact velocities, much greater than the characteristic velocity of target electrons, all four particles have the same ionization cross section. Therefore in the high energy limit the cross sections should merge. At lower velocities the positive particles generally

have higher ionization cross sections, as expected from polarization effects. Electron-impact ionization differs from the other three collisions in the indistinguishability of the projectile and the target electrons. Exchange interaction is a part of Coulomb interaction, originating from specific correlation in the movement of electrons caused by the symmetry of the coordinate part of the electronic wave function. Mathematically, in the case of e^- and e^+ scattering the only difference in the ionization matrix element is the exchange term, which is absent for the proton impact. As for electrons of the target, they, of course, have exchange interaction in both cases. In Fig. 6.7 the
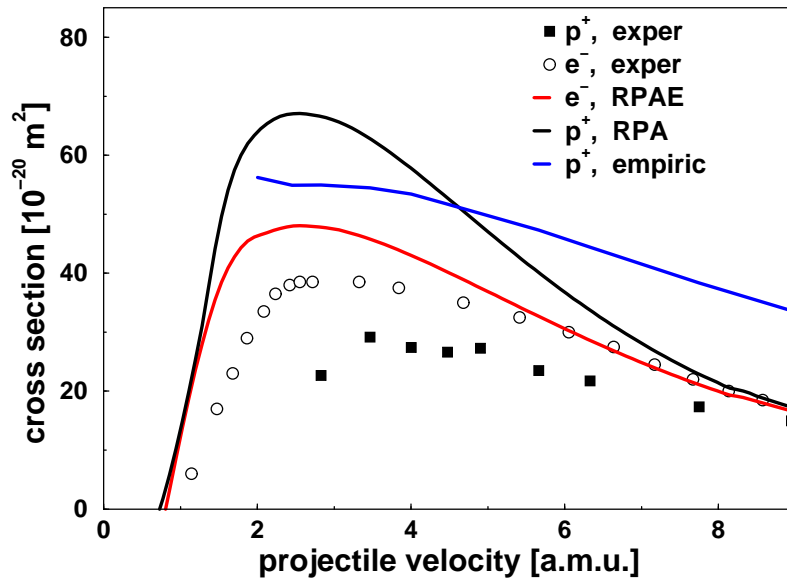

Figure 6.7: Electron and proton impact ionization of C_{60}: black curve – RPA calculations for proton impact; red curve – RPAE calculations for electron impact; filled symbols – experimental data for proton impact [86]; open symbols – experimental data for electron impact ionization of C_{60} [34, 58]; blue curve – calculations of [67] with one adjustable parameter.

single-ionization cross sections for electron- and proton-impact ionization of C_{60} are shown as a function of the projectile velocity (in atomic mass units). The polarization

of the fullerene molecule is accounted by RPAE. The electron-hole excitations are accounted by summation over all possible states of the discrete and continuum spectra of C_{60} obeying the energy conservation. As discussed above, at high impact energy $\sim 1\ keV$ the two curves begin to merge. At the intermediate energies due to different polarization of the fullerene by proton and electron, the difference between the cross sections is most prominent and maximal at $\sim 170\ eV$, where the curves differ by $\sim 30\%$. Interesting to note very close low-energy behavior of the cross sections.

Chapter 7

Single and multiple photoionization of fullerene

In this chapter we consider the single and multiple photoionization processes in a single fullerene molecule. The diffraction of the photoelectron wave on the fullerene shell, displaying itself in the oscillations of the photoionization cross section, is discussed. We calculate the ionization probabilities within the Hartree-Fock and frozen-core approximations. For the description of multiple photoionization, statistical energy deposition (SED) model is used in addition. The advantage of the SED model is that it is simple enough to be applied to the polyatomic systems, where more elaborate calculations are hardly feasible. As a result, different multiple photoionization cross sections of C_{60} in the photon energy range ~ 10 - $250\ eV$ are compared and analyzed, their order of magnitude is estimated.

7.1 Single photoionization

It is well known that the collision time with photons is much shorter than the characteristic time of any vibrational motion of the molecule. To a good approximation one can assume that photon transfers energy to a fixed in space molecule. In the sudden approximation, the wave function of the N-electron system, irradiated by the photon field, is represented as a product of the wave function of the ionized electron and the $(N-1)$-electron wave function of the other electrons:

$$\Psi(x_1, ..., x_{N-1}, x_N) = \psi(x_N)\Phi(x_1, ..., x_{N-1}), \tag{7.1.1}$$

The photoionization cross section as a function of the photon energy E_{ph} is given by

$$\sigma(E_{ph}) = 4\pi^2 \frac{e^2}{\hbar c} \hbar\omega |\mathbf{er}_{fi}|^2, \tag{7.1.2}$$

where ω and $\mathbf{e}$ are the photon frequency and polarization vector, respectively. The photoionization matrix element $\mathbf{r}_{fi}$ in the length form

$$\mathbf{r}_{fi} = \left\langle \psi_f \left| \mathbf{r} \right| \psi_i \right\rangle \tag{7.1.3}$$

describes the transition of the electron from the bound state ψ_i to the continuum state ψ_f. If the latter are the eigenstates of the spherically symmetric potential, i.e. have the form $\psi = u_\ell(r)Y_{lm}(\Omega)/r$, one can reduce the matrix element to an integral over the radial wave functions times a product of three spherical harmonics:

$$r_{fi}^{(\nu)} = \int_0^\infty u_{\ell_f}^*(r)\, r\, u_{\ell_i}(r)\, dr \sqrt{\frac{4\pi}{3}} \int d\Omega Y_{l_f m_f}^*(\Omega) Y_{1\nu}(\Omega) Y_{l_i m_i}(\Omega), \quad \nu = 0, \pm1. \tag{7.1.4}$$

For the calculation of the single photoionization of C_{60} we used one-electron Hartree-Fock wave functions of the shifted-square-well potential, described in the previous chapter. One of the features of the photoionization cross section of C_{60},

discussed in the literature (see e.g. [11, 68, 36]) and related to this particular shape of the confining potential, is the diffraction of the photoelectron waves between the well boundaries. In a simplified picture, if we forget for the moment about the Hartree-Fock corrections to the one-electron potential, the photoelectron wave emitted from the origin meets on its way to infinity two sharp potential edges, where it can absorb a photon. Consequently, there will be four resonant frequencies in the photoionization cross section (see discussion in [36]).

Indeed, the oscillations in the photoionization cross section are clearly visible (Fig. 7.1). However, smoothing of the abrupt potential edges by the mean-field electronic density smears out the idealized four-frequency behavior. The results of the
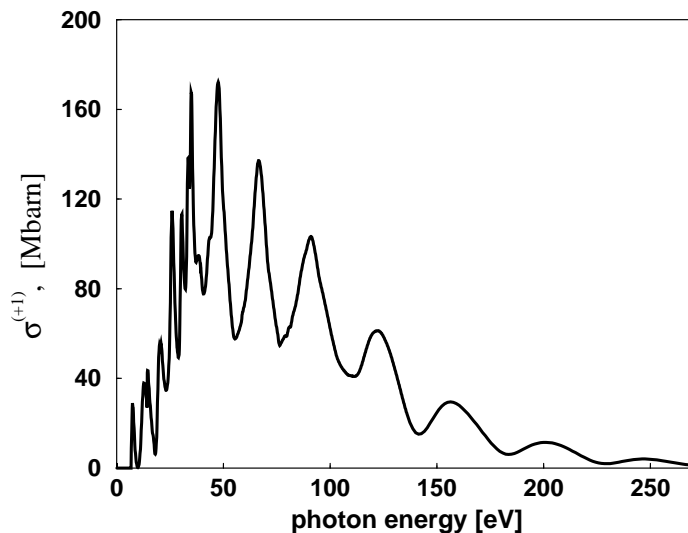

Figure 7.1: Single photoionization cross section of the highest occupied C_{60} orbital, present calculations.

calculations, presented in Fig. 7.1, correspond to the photoionization of the highest occupied orbital with energy $E_{HOMO} \sim -7.1 \, eV$. Despite the simplicity of the model, the theoretical curves are in good agreement with the available experimental data,
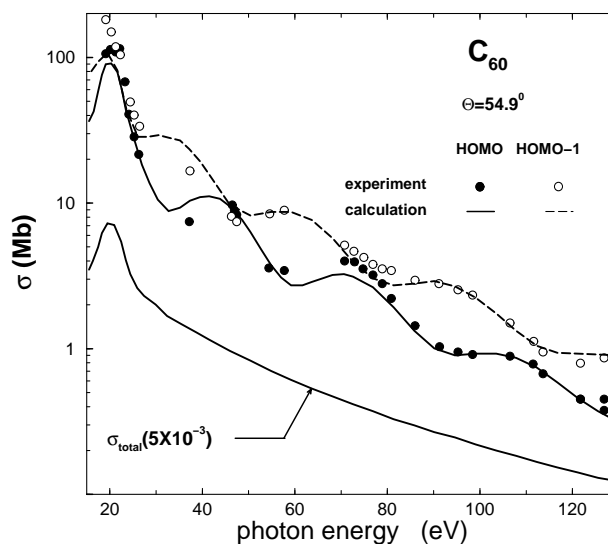
Figure 7.2: Experimental partial cross-sections of the highest occupied molecular orbitals $HOMO$ and $HOMO$-1 of C_{60} with a total photoionization cross-section (taken from [11]).

see Fig. 7.2 (note the logarithmic scale there).

7.2 Multiple photoionization

Upon photoionization the photon energy is transferred to the electronic degrees of freedom of the target. The deposited energy is partly spent for ionization (binding energy of electrons and their kinetic energy). However, some part of the deposited energy is transferred to the vibrational degrees of freedom, i.e. to the internal energy of the molecular ion. The subsequent dissociation of the excited molecular ion may include emission of photons, delayed electrons or small fragments. A theoretical description of the photo- and electron-induced multiple ionization is complicated mainly due to the variety of mechanisms that may contribute to it as well as its multielectron nature, strongly related to electron-electron correlations. In addition to the direct knock-out of electrons, processes such as shake-off, fast Auger cascades

after inner-shell ionization, excitation and multiple excitations followed by autoion-
ization can contribute. Due to the complexity of the problem, to the best of our
knowledge there is no theoretical description of the process of multiple photoioniza-
tion of fullerenes. However, in the field of ion-fullerene collisions there exists a model,
adopted from the early stage of investigation of atomic multiple ionization [67]. This
model, referred to as statistical energy-deposition model (SED) [73, 74, 71, 70, 72],
implies that the process is viewed to proceed in two stages. First, part of the kinetic
energy of the projectile is transferred to electronic excitations of the target atom. In
the second stage, the deposited energy is distributed among all target electrons and
the system subsequently autoionizes to reach its final ionization state. In the case of
collisions with charged particles, the deposited energy is considered as a fluctuating
quantity [67], characterized by a certain distribution, and the ionization probability
is then calculated as a weighted average over this distribution. Adapted to the mul-
tiple photoionization, the deposited energy is well defined at is equal to the photon
energy. Then the probability of n-fold ionization for certain deposited energy E_{ph} can
be expressed as

$$P_n^{(N)}(E_{ph}) = \frac{C_N^n g^n S_n(E_k/\varepsilon_1)}{\sum_{i=1}^{N} C_N^i g^i S_i(E_k/\varepsilon_1)}. \tag{7.2.1}$$

Here N is the total number of target electrons, C_N^n is the binomial coefficient, and
E_k is the kinetic energy carried off by the photoelectrons if the residual ion is left in
the n-th ionization state. The energy conservation implies that

$$E_k = E_{ph} - \sum_{i=1}^{n} \varepsilon_i - E_R(n), \tag{7.2.2}$$

where $E_R(n)$ is the residual excitation of the ion and ε_i is the i-th ionization energy. Parameter g is proportional to the mean-square matrix element of a single ionization and it is supposed that for multiple ionization the mean-square matrix element behaves according to the power law.

For the factor $S_n(E_k/\varepsilon_i)$ characterizing the density of final states a simple expression was obtained [72]:

$$S_n(E_k) = 2^{\{(n-1)/2\}}\pi^{\{n/2\}}E_k^{(3n-2)/2}/(3n-2)!! \ , \tag{7.2.3}$$

where $\{a\}$ stands for the integer part of a. All possible ways to reach the final state with n electrons in the continuum are considered as being equivalent. For example, inner-shell ionization followed by fast Auger process is also included into consideration.

In [72, 67] the SED model was used in a semiphenomenological way in a sense that the mean-square matrix element g was considered as a (free) parameter. In our calculations we extend the model in this respect. Namely, we calculate the single photoionization matrix element of the fullerene cluster in the Hartree-Fock approximation (c.f. Sec. 7.1). Here it is assumed that removal of the electron(s) from the single-particle Hartree-Fock levels does not affect the states of the remaining electrons, i.e. the fullerene ion has zero residual excitation energy E_R. In more elaborate calculations using RPAE this step may be further improved, since then the energy conservation requirement will imply certain energy spent to the electronic excitations of the residual ion.

Examples of the multiple photoionization of the highest occupied fullerene state are given in Fig. 7.3. One can note that the qualitative and quantitative behavior of the presented double, triple and 5-fold ionization cross sections is determined by

several circumstances. The oscillations in the cross sections are due to the oscillating nature of the single photoionization matrix element (c.f. Fig. 7.1), i.e. it is a consequence of the interference of the electronic waves within the fullerene shell. The dependence on the n-th power of the SPI square matrix element in the expression for the probability Eq. (7.2.1) makes the oscillations more pronounced when going to larger n. Difference in the order of magnitude for different n is mainly governed by the denominator in Eq. (7.2.3), making the n-fold ionization rapidly decreasing with increasing n. Note also the difference in the orders of magnitude of the cross sections for different n. For example, the double photoionization of C_{60} is approximately factor 20 less probable than the single photoionization. The possibility to estimate the order of magnitude of different multiple ionization processes can be viewed as a main practical achievement of the present calculations.
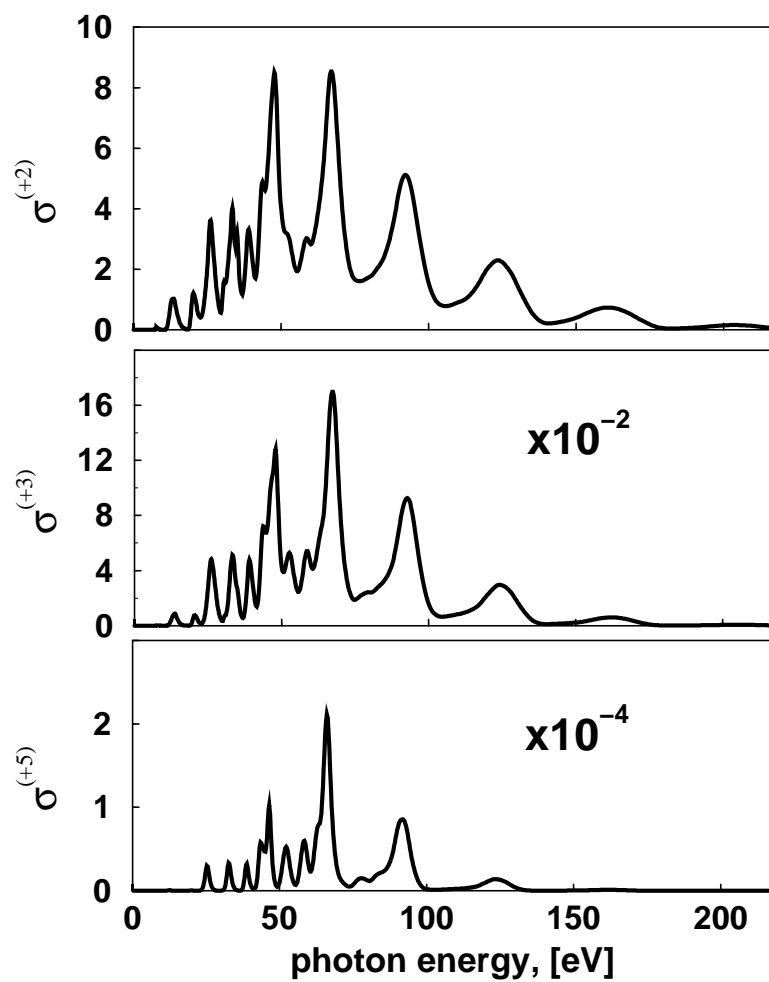
Figure 7.3: Double, triple and 5-fold photoionization cross sections of C_{60}, calculated in the SED model and in the HF approximation.

Chapter 8

Double photoionization of quantum dots and metal clusters

Semiconductor quantum dots and metal clusters have similar electronic structure, which to a good approximation can be modelled by an oscillator potential [25, 42]. In this chapter we use the exact two-electron states of the parabolic potential well to calculate the double photoionization (DPI) spectra of such nanoparticles. Being exactly solvable, the problem of two electrons coupled by Coulomb interaction in the oscillator confinement provides a unique test for any approximate theories, dealing with the few-body systems and the related experiments. An instructive treatment based on a direct mapping of a two-electron initial state density onto the DPI observables is proposed, which clearly explains how the DPI spectra are organized and gives useful hints for possible experimental measurements.

8.1 Double photoionization

Evaluation of the effects of electronic correlations has to be included in most of the theories dealing with the electronic excitations by external fields. While for some processes (e.g. single photoemission [41, 56]) the account of correlations leads only to a refinement of the calculated transition probabilities (which otherwise can be calculated in the independent-electron approximation), for some other processes (e.g. [12, 59]) it is a vital ingredient of the theoretical description, playing a major role in determining the characteristics of the process. In the latter case the careful use of approximations is important, for it can happen that the features introduced by some aggressive approximations may become even more pronounced than those, inherent to a very physical process. Therefore, it is important to have a reference among the exactly solvable models to be able to judge the quality of the approximate solutions.

One such process, which occurs as a result of the electron-electron interaction and is impossible in the independent-electron picture [12], is the double photoionization (DPI). In DPI the absorption of a photon by a system results in the simultaneous emission of a pair of electrons. In a schematic way it can be described by a diagram, Fig. 8.1, where the bold line represents the exact two-electron initial and final states Φ_2 and Ψ_2, respectively, wavy line depicts a photon with energy ω_{ph}. For a particular case of a parabolic potential well the two-electron eigenstates can be found without approximations [82, 83]. Physical systems showing the electronic structure, well reproduced by the oscillator confinement, are the semiconductor quantum dots [42] or metal clusters [?]. Here for concreteness we consider the DPI from a single quantum dot.
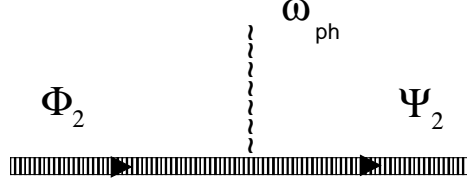
Figure 8.1: Diagrammatic representation of DPI: two-particle state Φ_2 evolves into the two-particle state Ψ_2 by absorbing photon with the energy ω_{ph}.

8.2 Exact solution

For the description of a semiconductor medium we assume the effective mass approximation (m^* is taken in units of the bare electron mass) and the weakening of the Coulomb interaction by the static dielectric constant ϵ. Atomic units are used throughout.

Upon the transformation to the center-of-mass and relative coordinates

$$\mathbf{R} = \frac{1}{2}\left(\mathbf{r}_1 + \mathbf{r}_2\right), \, \mathbf{r} = \mathbf{r}_1 - \mathbf{r}_2, \tag{8.2.1}$$

the Hamiltonian for two interacting electrons in the parabolic well

$$H = -\frac{1}{2m^*}\nabla^2_{r_1} - \frac{1}{2m^*}\nabla^2_{r_2} + \frac{1}{2}m^*\omega^2{r_1}^2 + \frac{1}{2}m^*\omega^2{r_2}^2 + \frac{1}{\epsilon\left|\mathbf{r}_1 - \mathbf{r}_2\right|}. \tag{8.2.2}$$

can be expressed as a sum of two independent parts:

$$H = -\frac{1}{4m^*}\nabla^2_R - \frac{1}{m^*}\nabla^2_r + \frac{m^*}{4}\omega^2 r^2 + m^*\omega^2 R^2 + \frac{1}{\epsilon r} \equiv H_R + H_r, \tag{8.2.3}$$

with the two-electron wave function being also separable in these coordinates:

$$\Phi_2\left(1, 2\right) = \varphi\left(\mathbf{r}\right) \cdot \xi\left(\mathbf{R}\right) \cdot \chi\left(s_1, s_2\right). \tag{8.2.4}$$

The total energy is then given by the sum of the eigenenergies E_R and E_r of H_R and

H_r, respectively:

$$E = E_R + E_r. \tag{8.2.5}$$

As is usual for the spin-independent Hamiltonians, the Pauli principle is guaranteed in that the spin part of the wave function $\chi(s_1, s_2)$ has to be chosen symmetric or antisymmetric (with respect to particle exchange) in accordance with the symmetry of its coordinate part. The Schrödinger equation for the *center-of-mass* (CM) motion coincides with the equation for the 3D harmonic oscillator

$$\left[-\frac{1}{2m^*}\nabla_{\mathbf{R}}^2 + \frac{1}{2}m^*\omega_R^2 R^2 \right] \xi(\mathbf{R}) = E_R'\xi(\mathbf{R}),\ \omega_R \equiv 2\omega,\ E_R' \equiv 2E_R, \tag{8.2.6}$$

and has analytical solutions [33], classifiable according to the node number N and orbital momentum quantum number L

$$\xi_{NLM}(\mathbf{R}) = \frac{U_{NL}(R)}{\sqrt{m^*}R}Y_{LM}(\hat{\mathbf{R}}),\ N = 0, 1, 2...,\ L = 0, 1, 2..., \tag{8.2.7}$$

where the radial function is given in terms of the confluent hypergeometric functions [1]

$$U_{NL}(R) = (\sqrt{m^*}R)^{L+1}\exp\left(-\frac{m^*\omega}{2}R^2\right)F\left(-N, L+\frac{3}{2}; m^*\omega R^2\right). \tag{8.2.8}$$

The equation for the *relative* motion, like the one for the CM motion, also possesses a spherical symmetry:

$$\left[-\frac{1}{2m^*}\nabla_{\mathbf{r}}^2 + \frac{1}{2}m^*\omega_r^2 r^2 + \frac{1}{2\epsilon r} \right] \varphi(\mathbf{r}) = E_r\varphi(\mathbf{r}),\ \omega_r \equiv \frac{1}{2}\omega,\ E_r' \equiv \frac{1}{2}E_r. \tag{8.2.9}$$

It's eigenstates are classified in the same way as the oscillator wave functions (8):

$$\varphi_{n\ell m}(\mathbf{r}) = \frac{u_{n\ell}(r)}{\sqrt{m^*}r}Y_{\ell m}(\hat{\mathbf{r}}),\ n = 0, 1, 2...,\ \ell = 0, 1, 2... . \tag{8.2.10}$$

The radial function $u_{n\ell}(r)$ is a solution of the radial Schrodinger equation

$$\left[-\frac{1}{2m^*}\frac{d^2}{dr^2} + \frac{1}{2}m^*\omega_r^2 r^2 + \frac{1}{2}\frac{1}{\epsilon r} + \frac{\ell(\ell+1)}{2m^*}\frac{1}{r^2} \right] u_{n\ell}(r) = \epsilon' u_{n\ell}(r), \qquad (8.2.11)$$

which can be integrated numerically and in some special cases has analytical solution [82].

Summarizing this part, the motion of the pair of electrons is described by independent motions of two quasi-particles, described by the wave functions $\xi(\mathbf{R})$ and $\varphi(\mathbf{r})$ and moving in $\mathbf{R}-$ and $\mathbf{r}-$subspaces, respectively. The two-electron wave function is defined by six quantum numbers (N, L, M, n, ℓ, m). The ground state of the two-particle system is constructed from the ground states of the quasi-particles, the excited state is reached whenever any or both of the motions are excited. For simplicity, in the following we restrict our calculations by the quasi-particle wave functions with $M=m=0$. In Fig. 8.2 the two-electron wave function characterized by different combinations of (N, L, n, ℓ) is shown as a function of (r, R). The number of extrema corresponding to a different degree of excitation of the CM and 'relative' motions can be easily seen. The calculations are made for the confinement frequency $\omega = 0.32\ a.u.$ Then the spatial extent of the ground state wave function is of the order of 100Å, which is, in turn, of the order of a typical size of a quantum dot. We used GaAs effective mass and dielectric constant ($m^* = 0.067$, $\epsilon = 12.4$).

8.3 DPI probability

In the dipole approximation, the DPI amplitude describing the photon-induced transition between two-electron initial and final states reads:

$$T = \langle \Psi_2 | \mathbf{e} \cdot (\nabla_1 + \nabla_2) | \Phi_2 \rangle, \qquad (8.3.1)$$
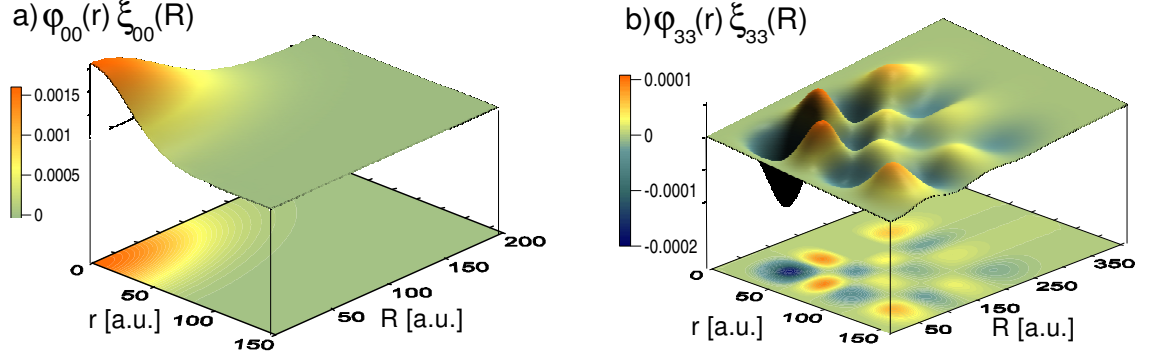
Figure 8.2: Ground $(0,0,0,0)$ and excited $(3,3,3,3)$ two-particle states of a quantum dot (for it's parameters see text) in the CM and relative coordinates.

where $\mathbf{e}$ is the photon polarization vector, $(\nabla_1 + \nabla_2)$ is a two-particle dipole operator in the velocity form.

Although the representation of a quantum dot or metal cluster potential in the form of the infinite harmonian is an idealization, we assume that its low-lying eigenstates reproduce the two-electron states of the real systems qualitatively correctly. Such approximation significantly simplifies the description of the initial state wave function Φ_2, since for the finite oscillator well the same problem loses separability.

To single out the effect of the initial state correlations, we start from the simplest two-electron final state, constructed as a product of plane-wave asymptotic detector states: $\left| \Psi_2 \right\rangle = \left| \mathbf{k_1} \right\rangle \otimes \left| \mathbf{k_2} \right\rangle$. The physical justification of this approximation is that after the emission of electrons quantum dot becomes quickly neutralized by the substrate, so that the final-state three-body interaction between two electrons and an ion effectively reduces to a two-body interaction between electrons. With this approximation, the DPI amplitude factorizes in $(\mathbf{r}, \mathbf{R})$ space and reduces to the

product of the Fourier-transformed wave functions for the CM and relative motion:

$$
\begin{aligned}
T_{\mathbf{k}_1\mathbf{k}_2} &= \left\langle \mathbf{k}_1, \mathbf{k}_2 \middle| \mathbf{e} \cdot (\nabla_1 + \nabla_2) \middle| \Phi_2 \right\rangle = \\
&= \langle \mathbf{k}_1 + \mathbf{k}_2 | \mathbf{e} \cdot \nabla | \xi(\mathbf{R}) \rangle \cdot \langle (\mathbf{k}_1 - \mathbf{k}_2)/2 | \varphi(\mathbf{r}) \rangle = \\
&= \mathbf{e} \cdot \mathbf{Q} \; \widetilde{\xi}(\mathbf{Q}) \; \widetilde{\varphi}(\mathbf{q}),
\end{aligned}
\tag{8.3.2}
$$

where we have introduced CM and 'relative' momenta $\mathbf{Q} = \mathbf{k}_1 + \mathbf{k}_2$ and $\mathbf{q} = (\mathbf{k}_1 - \mathbf{k}_2)/2$, wavy line denotes the Fourier transform, ∇ is a two-electron momentum operator in $(\mathbf{r}, \mathbf{R})$ space. In Fig. 8.3(a,b) we plot the square modulus of the transition amplitude as a function of (q, Q). The number of nodes of the wave function in the momentum space is the same as in the configuration space, therefore the number of maxima in Fig. 8.3(a,b) can be easily identified with the quantum numbers n and N of the corresponding wave functions.

Next, to simulate final state two-body Coulomb interaction, we introduce the two-electron density of final states in the form $\rho(\mathbf{k}_1, \mathbf{k}_2) = \rho(q) = 2\pi\alpha/(\exp(2\pi\alpha) - 1)$, $\alpha = \frac{1}{2|\mathbf{q}|}$ [43]. It monotonously suppresses the emission of the pairs, having small relative momentum, and 'blows off' the positions of the maxima of $|T_{\mathbf{k}_1\mathbf{k}_2}|^2$ towards higher $\mathbf{q}$, as can be seen from Fig. 8.3(c,d).

Finally, apart from a constant normalization factor, 6-fold differential DPI cross section reads:

$$
\begin{aligned}
\frac{d\sigma}{dE_1 dE_2 d\Omega_1 d\Omega_2} &\sim |T_{\mathbf{k}_1\mathbf{k}_2}|^2 \; \rho(\mathbf{k}_1, \mathbf{k}_2) \; \delta(E_R + E_r + \hbar\omega - E_1 - E_2) = \\
&= \left| \mathbf{e} \cdot \mathbf{Q} \, \widetilde{\xi}(\mathbf{Q}) \right|^2 \cdot \left| \widetilde{\varphi}(\mathbf{q}) \right|^2 \rho(\mathbf{q}) \; \delta(E_R + E_r + \hbar\omega - E_1 - E_2).
\end{aligned}
\tag{8.3.3}
$$

Note that the photon transition is contained entirely in the CM part, while the effects of electronic correlation are included only in the 'relative' part of the cross section. Evident experimental use of this factorization is that keeping one of the vectors, $\mathbf{Q}$ or
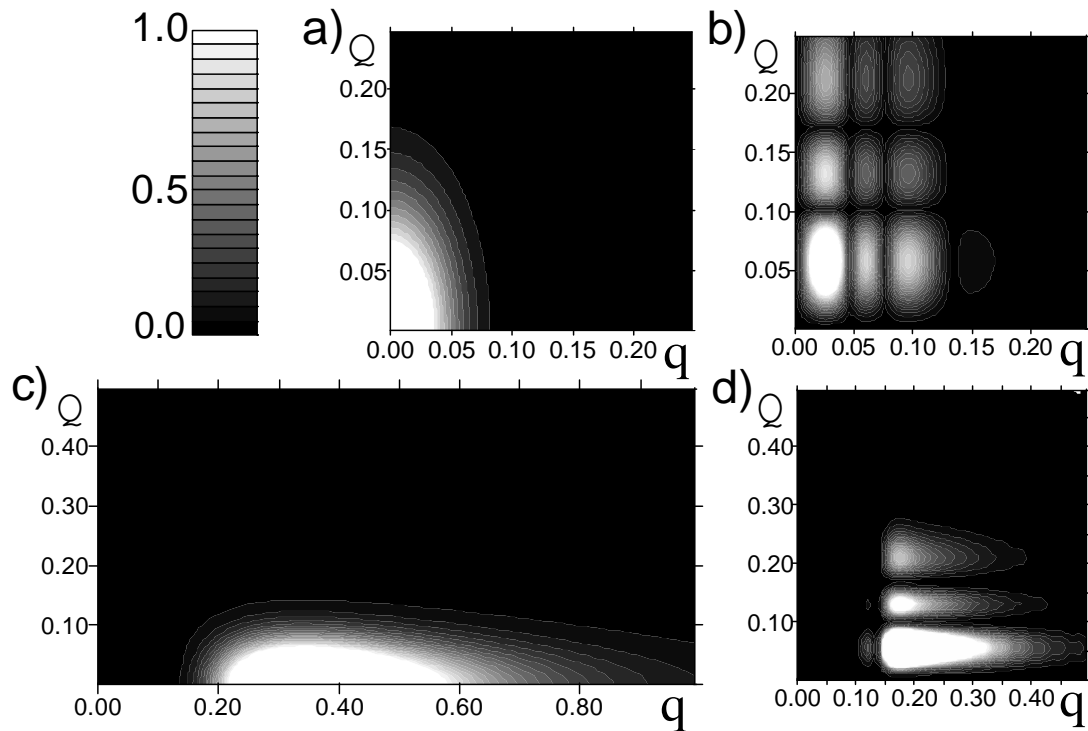
Figure 8.3: Momentum distribution of a two-particle state in the CM and relative coordinates: (a),(b) - ground state and excited (2,2,2,2) state; (c),(d) - the same but multiplied by the density of final states $\rho(\mathbf{k}_1, \mathbf{k}_2)$. Black-and-white scale corresponds to zero-to-one intensity scale.

q, fixed, one can investigate the behavior of the DPI cross section separately either with respect to correlations, or with respect to the dipole transition.

Let us mention the properties of the transition amplitude, Eq. (8.3.1).

- First, the scalar product $\mathbf{e} \cdot (\mathbf{k}_1 + \mathbf{k}_2)$ in Eq. (8.3.1) originates from the approximation used for the final state and serves as a selection rule when $\mathbf{e} \cdot (\mathbf{k}_1 + \mathbf{k}_2) = 0$. The electrons, which are emitted with $\mathbf{k}_1 = -\mathbf{k}_2$, or whose total momentum is normal to the polarization vector $\mathbf{e}$, will not contribute to the cross section.

- Second, the CM wave function $\xi(\mathbf{R})$ is always symmetric with respect to particle exchange. Therefore the singlet (triplet) spin part for the two-electron state has to be taken whenever $\varphi(\mathbf{r})$ is even (odd) function. The latter, in turn, is fully specified by the orbital quantum number ℓ in Eq. (8.2.10): even (odd) ℓ's correspond to singlet (triplet) two-electron states. From this we note another selection rule: two electrons in the triplet state can not be emitted with $\mathbf{k}_1 = \mathbf{k}_2$. This is just a consequence of the Pauli principle.

- Third property of the transition amplitude arises from the symmetry constraints on the dipole transition. Namely, the single photoionization dipole selection rules [4, 37] are valid for the matrix element $\langle \mathbf{k}_1 + \mathbf{k}_2 | \mathbf{e} \nabla | \xi(\mathbf{R}) \rangle$. For the given quantum numbers (L, M) of the $\xi_{NLM}(\mathbf{R})$, only components of the final-state CM plane wave with the orbital momenta $L' = L \pm 1$ will be selected. The magnetic quantum numbers M and M' of initial and final CM states will be connected through the polarization of the photon: $M + \mu = M'$ (the projection of the photon angular momentum $\mu = 0$ for linear and $\mu = \pm 1$ for circular polarization).

- It is only the relative motion that depends on the interaction between electrons.
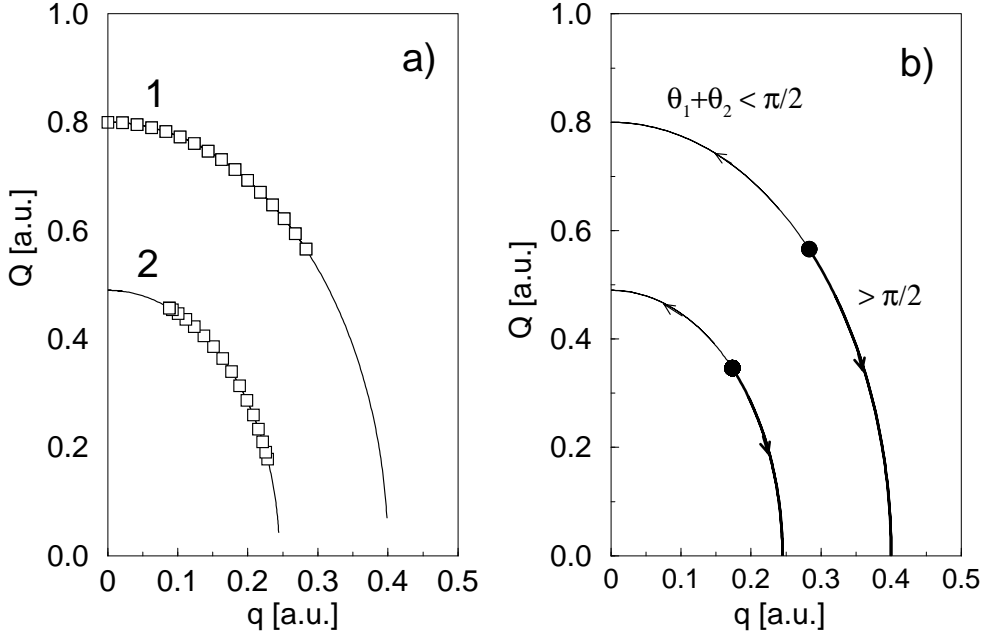
Figure 8.4: a): Location of (q, Q) final state momenta contributing to the angular distributions. Curve 1. $E_{tot} = 0.16$ *a.u.*, $E_1 = E_2$, full line: $\theta_2 = 80^0$, squares: $\theta_2 = 0^0$. Curve 2. $E_{tot} = 0.06$ *a.u.*, $\theta_2 = 80^0$, full line: $E_1 = E_2$, squares: $E_1 \neq E_2$. b): Location of (q, Q) final state momenta contributing to the energy sharing distributions. Curves 1 and 2 correspond to $E_{tot} = 0.16$ *a.u.* and $E_{tot} = 0.06$ *a.u.*, respectively. Black point corresponds to $\theta_1 + \theta_2 = 90^0$, left(right) arrow shows the direction of changing the (q, Q)-momenta participating in ESD with decrease(increase) of $\theta_1 + \theta_2$.

Varying the strength of this interaction leads to the change of the shape of the potential well in Eq. (8.2.8) and causes the corresponding change of the localization of $\varphi(\mathbf{r})$ and $\tilde{\varphi}(\mathbf{q})$: the more strong is the Coulomb interaction, the more localized becomes the momentum density distribution along q-coordinate.

8.4 Angular distributions

We present the results in the form of angular (AD) and energy sharing (ESD) distributions. In the first case, the DPI cross section is plotted as a function of emission
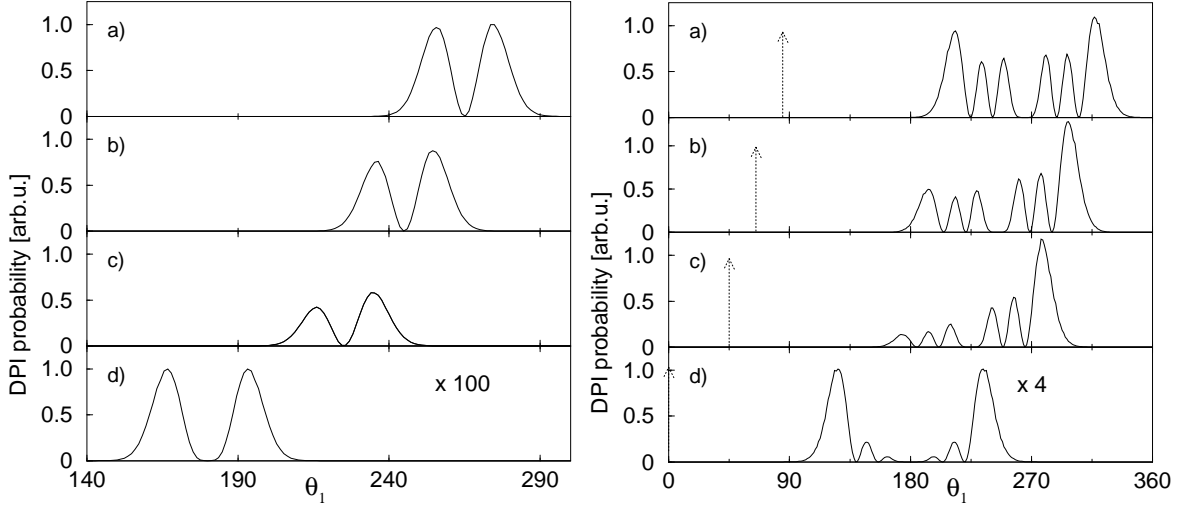
Figure 8.5: ADs from the ground (left panel, $E_{tot} = 0.16$ $a.u.$) and excited (2,2,2,2) states (right panel, $E_{tot} = 0.06$ $a.u.$) for different θ_2. Plots (a)-(d) correspond to $\theta_2 = 85^0, 65^0, 45^0, 0^0$, respectively. Dotted arrow marks the emission direction of the 'fixed' electron, light is polarized along the $(0^0, 0^0)$ direction. $E_1 = E_2 = E_{tot}/2$.

angles (θ_1, ϕ_1) of one electron at fixed emission angles (θ_2, ϕ_2) of the second electron and fixed final state energies E_1 and E_2. In the second case, the DPI cross section is given as a function of the energy difference $(E_1 - E_2)$ for fixed emission directions and fixed total energy $E_{tot} = E_1 + E_2$. We assume that electron detectors are always placed in the azimuthal plane, i.e. azimuthal emission angles are $\phi_1 = \phi_2 = 0^0$. Polarization vector $\mathbf{e}$ of linearly polarized light is chosen along $(\theta_{ph}, \phi_{ph}) = (0^0, 0^0)$ direction.

Before coming up to the results, it is helpful to visualize the distribution of the final-state momenta, taking part in ADs and ESDs, Fig. 8.4a and 8.4b, respectively. The relation between the wave vectors $\mathbf{Q}$ and $\mathbf{q}$ implies, that points with coordinates (q, Q), corresponding to a fixed total final-state energy $E_{tot} = (k_1^2 + k_1^2)/2$, are located on a quarter of an ellipse. The length of it's axes differs by factor 2 due to the difference in the scaled oscillator frequencies, c.f. Eq. (8.2.5) and (8.2.8). Curves 1

and 2 correspond to $E_{tot} = 0.16$ *a.u.* and $E_{tot} = 0.06$ *a.u.*, respectively. Depending on the experimental setup, final states with momenta $(\mathbf{q}, \mathbf{Q})$ arising from the different parts of the ellipse participate in the angular distribution. For example, solid lines in Fig. 8.4a depict the pairs (q, Q), corresponding to the grazing emission angle for the 'fixed' electron $(\theta_2 = 80^0)$, while the first electron is emitted in the range $\theta_1 = 0^0 \dots 180^0$. Kinetic energies of the two electrons are equal. By decreasing angle θ_2, the participating arch of the ellipse is made shorter, e.g. at normal emission of the 'fixed' electron $(\theta_2 = 0^0)$ only the part of the ellipse, shown by squares in curve 1, is left. Making the kinetic energies of the electrons unequal also cuts off the part of the ellipse. In curve 2 the solid line corresponds to $E_1 = E_2 = 0.03$ *a.u.*, the square symbols show the range (q, Q) for $E_1 = 0.01$ *a.u.*, $E_2 = 0.05$ *a.u.* (for $\theta_2 = 80^0$, $\theta_1 = 0^0 \dots 180^0$). Using these parameters (total kinetic energy, it's distribution between electrons, angle of emission) as levers, one can tune through any required region on a (q, Q) map.

To probe the ground state (c.f. Fig. 8.3(c)), we chose $E_{tot} = 0.16$ *a.u.* (curve 1, Fig. 8.4a). In Fig. 8.5, left panel, ADs for different $\theta_2 = 85^0, 65^0, 45^0, 0^0$ and for $E_1 = E_2 = E_{tot}/2$ are presented. Two maxima on the ADs originate from a single maximum in the ground state wave function, damped in the middle by the factor $\mathbf{e} \cdot (\mathbf{k}_1 + \mathbf{k}_2)$, which becomes equal to zero at $\theta_1 = \pi + \theta_2$. Another example is shown in Fig. 8.5, right panel: for the same choice of angles and for $E_{tot} = 0.06$ *a.u.* (curve 2, Fig. 8.4a) we plot the DPI ADs from the initial two-particle state (2,2,2,2)(c.f. Fig. 8.3(d)).

8.5 Energy sharing distributions

ESD shows how the DPI probability depends on the difference between individual kinetic energies of two electrons, at all the other parameters fixed. First, we note that if the angle between outgoing electrons is equal to $\pi/2$, only one point on the (q, Q)-map contributes to the cross section (see Fig. 8.4b, black point). By decreasing or increasing the relative angle, the arches to the left or to the right from this point become 'visible', as is shown in Fig. 8.4b. In Fig. 8.6, left panel, this trend is shown for the case of emissionionization from the (2,2,2,2)-state. The angle between electrons is decreasing ($\theta_1 = -\theta_2 = 85^0, 75^0, 55^0, 45^0$), that gradually excludes the maxima of the initial-state density out of the allowed (q, Q)-region. This shows up in vanishing of the oscillations in the ESDs, and also in decrease of its magnitude. In Fig. 8.6, right panel, the role of choice of E_{tot} is demonstrated for the ionization from the ground state. Scanning through the single maximum on a (q, Q)-map results in the change of the intensity of the sharing distribution without changing it's shape. The minimum in the middle of ESD is again due to the selection rule, when at equal energies vector $(\mathbf{k}_1 + \mathbf{k}_2)$ becomes normal to the polarization vector of light.

In conclusion, we note that the reconstruction of the two-electron density on the (q, Q)-grid, using experimental data, would be straightforwardly tractable in the frames of given approach. Obviously, the present problem can be generalized to another forms of electron-electron interaction, dependent only on the distance between the electrons.
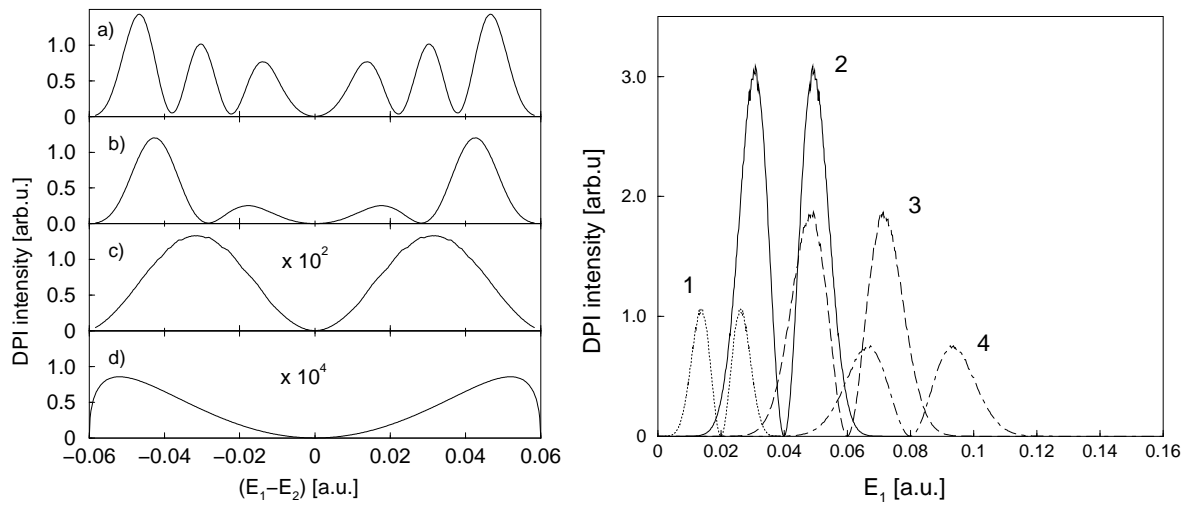
Figure 8.6: ESDs from the excited (2,2,2,2) (left panel) and the ground (right panel) state. Plots (a)-(d), left panel, correspond to $\theta_1 = \theta_2 = 85^0, 75^0, 55^0, 45^0$. Four curves on the right panel correspond to $E_{tot} = 0.04, 0.08, 0.12, 0.16\ a.u.$ (note different abscissas in the left and right panels).

Chapter 9

Conclusions

In the present work we investigated the correlation effects in the alkali-metal clusters, fullerenes and semiconductor quantum dots. Both approximate many-body methods and exactly solvable problems were employed for the description of the electronic structure of the systems under study. We use the HF theory as a basis for the systematic account of electron-electron interactions in the perturbative framework, which was performed in the random phase approximation.

Application of the Hartree-Fock formalism to the systems with the large number of electrons, although formally established, represents severe technical difficulties due to the presence of a huge number of the nonlocal exchange integrals. To increase the efficiency of such calculations, we developed a new conceptual framework, based on the extension of the variable phase approach to the nonlocal potentials and showed how the Hartree-Fock problem is reformulated in terms of our method. We also proposed the efficient finite-difference scheme for its numerical implementation. The advantage of this scheme stems from the fact that for the calculation of the Hartree-Fock integrals only the diagonal part of the nonlocal one-electron potential is required.

We would like to emphasize that this is a property of the variable phase approach rather than a consequence of any approximations.

The ionization of the many-electron system by a charged particle is a fundamental physical process, allowing a direct information on the correlated electron dynamics. The fluctuations of the electronic charge density of the clusters, accounted in the random phase approximation with exchange, were shown to suppress the single ionization channel in the low-energy region, while at large impact energies they are not essential. This tendency is in full agreement with the experimental data for fullerene clusters. In contrast, the calculations performed without the account of the dynamic screening were unable to reproduce the experimental data, giving a wrong low-energy behavior of the ionization cross section. Our first principle numerical results were interpreted with the help of the Thomas-Fermi model of screening. The qualitative conclusion of this study is that the change of the effective radius of the inter-electron interaction does not lead to a simple scaling of the ionization probability, as it could be supposed, but modifies also its energy dependence. In addition, we investigated the interplay between quantum size and nonlocal screening effects by tracing the changes in the ionization cross sections for Li clusters with an increasing cluster radius. The particle-hole excitations proved to play a decisive role in the evolution of the ionization cross sections of the clusters with the increase of their size and, consequently, with the increase of the number of delocalized electrons. Actually, we observed that the inclusion of the dynamic screening leads to the flattening of the ionization cross section as the cluster size grows, while the disregard of this phenomenon gives the opposite tendency. What is less obvious, the energy position of the maximum in the cross section also shifts in the opposite directions. Experimental measurements

clarifying these size effects would be very helpful.

A specific sort of correlations arising from the exchange interaction was traced via a comparison of the proton and the electron impact ionization of C_{60}. The absence of the exchange between the proton and the target electrons qualitatively plays the same role as the disregard of the particle-hole (de)excitations in the many-electron system. Namely, the $\sim 30\%$ increase of the proton impact ionization probability as compared to the electron impact was observed.

For the description of the multiple ionization of fullerenes by a single photon, the statistical energy deposition model was used for the first time. Usually, the calculations based on this model employed adjustable or semiempirical parameters for the estimation of the single ionization transition amplitude, which enters the expression for the multiple ionization probability. We improve this step by performing the first principle calculations of this quantity. In doing this we get a natural access to the material, structural and energy dependence of the multiple ionization processes. For the first time the probabilities of different multiple photoionization reactions in C_{60} were estimated and compared. The diffraction of the photoelectron wave on the fullerene shell was shown to be a prominent feature of these processes.

One of the few exactly solvable quantum-mechanical problems is the problem of two electrons, coupled via bare Coulomb repulsion, in the parabolic confinement. Using the exact two-electron wave function, the double photoionization cross section of a quantum dot was derived and the various angular and energy spectra were calculated. The mapping of the two-electron density onto the double photoionization spectra was suggested as a promising tool for the visualization of subtle correlation effects.

The results of this work may be applied to the problems dealing with the arbitrary nonlocal or momentum-dependent potentials, to the arbitrary systems of integro-differential equations and as a theoretical background for the experimental investigations of the influence of the quantum size effects on the strength of the electronic correlations.

Appendix A

Hartree-Fock equations

Consider the Hamiltonian of the a system of N electrons moving in an external confining potential V^{ion} and interacting through the Coulomb two-body potential

$$\widehat{H}_0 = \sum_{i=1}^{N} \left\{ - \bigtriangledown_i^2 + V^{ion}(\mathbf{r}_i) + \sum_{j \neq i}^{N} \frac{1}{|\mathbf{r}_i - \mathbf{r}_j|} \right\}. \tag{A.0.1}$$

The ground state wave function Ψ of an N-electron system is approximated by a Slater determinant constructed as an antisymmetrized product of orthogonal single-particle wave functions

$$\Psi(\mathbf{r}_1, \mathbf{r}_2 \ldots \mathbf{r}_N) = \frac{1}{\sqrt{N!}} \det \|\psi_i(\mathbf{r}_j, t)\|, \quad i, j = 1, 2, ..., N. \tag{A.0.2}$$

Obviously, Ψ satisfies the antisymmetrization condition, since the interchange of two particles is equivalent to the interchange of two lines (or two rows) of the determinant, which changes its sign.

According to the Ritz variational principle, the best possible wave function Ψ minimizes the mean value of the total energy of the system. The variation of the expectation value of the Hamilton operator (A.0.1) $\left\langle \Psi \left| \widehat{H}_0 \right| \Psi \right\rangle$ leads to the system

of the single-particle Hartree-Fock equations

$$- \triangle \psi_i(\mathbf{r}_i) + V^{ion}(\mathbf{r}_i) - k_i^2 \psi_i(\mathbf{r}_i) =$$
$$= - \sum_{j \neq i} \int d^3\mathbf{r}' \frac{\psi_j^*(\mathbf{r}')\psi_j(\mathbf{r}') - \psi_j^*(\mathbf{r}')\psi_j(\mathbf{r}_i)}{|\mathbf{r}_i - \mathbf{r}'|} \psi_i(\mathbf{r}'), \quad i = 1, \ldots, N \qquad (A.0.3)$$

Thus, the N-electron system is described by the system of N coupled integro-differential equations. The first term on the right-hand side of Eq. (A.0.3) represents the electrostatic potential for the i-th electron in the field of all other electrons. The second term is an integral operator, introducing a specific (exchange) correlation in the motion of the fermions, originating from their indistinguishability. The contributions from these two terms at $i = j$ compensate each other, thus preserving the electron from the interaction with itself.

Bibliography

[1] M. Abramowitz and I. Stegun, *Handbook of mathematical functions*, United States Department of Commerce, Washington, 1972.

[2] A. S. Alexandrov and C. J. Dent, J. Phys. C **13** (2001), L417.

[3] M. Ya. Amusia, A. S. Baltenkov, and U. Becker, Phys. Rev. A **62** (2000), 12701.

[4] M. Ya. Amusya, *Atomic photoeffect*, Plenum press, New York, 1990.

[5] N. W. Ashkroft and N. D. Mermin, *Solid state physics*, Saunders College Publ., Philadelphia, 1976.

[6] V. V. Babikov, JINR, Dubna, Preprint N2005 (1964), 28–32.

[7] _____, *Method of the phase functions in quantum mechanics*, Nauka, Moscow, 1968.

[8] K. L. Baluja and A. Jain, Phys. Rev. A **46** (1992), 1279.

[9] D. Bauer, F. Ceccherini, A. Macchi, and F. Cornolti, Phys. Rev. A **64** (2001), 63203.

[10] D. E. Beck, Phys. Rev. B **35** (1987), 7325.

[11] U. Becker, O. Gessner, and A. Rüdel, J. Electron Spectrosc. Relat. Phenom. **108** (2000), 189.

[12] J. Berakdar, Phys. Rev. B **58** (1998), 9808.

[13] G. F. Bertsch, A. Bulgac, D. Tománek, and Y. Wang, Phys. Rev. Lett. **67** (1991), 2690.

[14] J. L. Bohn, Phys. Rev. A **49** (1994), 3761.

[15] M. Brack, Rev. Mod. Phys. **65** (1993), 677.

[16] C. Bréchignac, *et al.*, Phys. Rev. Lett. **68** (1992), 3916.

[17] E. Brook, *et al.*, J. Phys. B **11** (1978), 3115.

[18] P. A. Brühwiller, *et al.*, Phys. Rev. B **48** (1993), 18296.

[19] F. Calogero, Nuovo Cimento **33** (1964), 352.

[20] _____, Nuovo Cimento **28** (1966), 66.

[21] _____, *Variable phase approach to potential scattering*, Academic Press, New York, 1967.

[22] E. Campbell and F. Rohmund, Rep. Prog. Phys. **63** (2000), 1061.

[23] I. Compagnon, *et al.*, Phys. Rev. A **64** (2001), 25201.

[24] J.-P. Connerade, *et al.*, J. Phys. B **32** (1999), 877.

[25] W. A. de Heer, Rev. Mod. Phys. **65** (1993), 611.

[26] W. A. de Heer, W. D. Knight, M. Y. Chou, and M. L. Cohen, Solid State Phys. **40** (1987), 93.

[27] H. Deutsch, *J. phys. b*, et al. **29** (1996), 5175.

[28] A. Domps, *et al.*, Phys. Rev. Lett. **81** (1998), 5524.

[29] P. Dugourd, *et al.*, Journal de Physique IV **1** (1991), 509.

[30] W. Ekardt, Phys. Rev. B **31** (1985), 6360.

[31] H. Faxén and J. Holtsmark, Z.Phys. **45** (1927), 307.

[32] A. L. Fetter and J. D. Walecka, *Quantum theory of many-particle systems*, McGraw-Hill, New York, 1971.

[33] S. Flügge, *Practical quantum mechanics*, Springer, Berlin, 1974.

[34] V. Foltin, *et al.*, Chem. Phys. Lett. **289** (1998), 181.

[35] L. Forró and L. Michály, Rep. Prog. Phys. **64** (2001), 649.

[36] O. Frank and J. M. Rost, Chem. Phys. Lett. **271** (1997), 367.

[37] H. Friedrich, *Theoretical atomic physics*, Springer, Berlin, 1998.

[38] L. G. Gerchikov, A. N. Ipatov, and A. V. Solov'yov, J. Phys. B **30** (1997), 5939.

[39] I. V. Hertel, *et al.*, Phys. Rev. Lett. **68** (1992), 784.

[40] N. P. Hohenberg and W. Kohn, Phys. Rev. B **136** (1965), 864.

[41] S. Hüfner, *Photoelectron spectroscopy: principles and applications*, Springer, Berlin, 1995.

[42] L. Jacak and A. P. Hawrylak, *Quantum dots*, Springer, Berlin, 1998.

[43] C. J. Joachain, *Quantum collision theory*, Elsevier, ..., 1979.

[44] K. Kawamura and M. Eto, Phys. Rev. B **51** (1995), 10119.

[45] S. Keller, Eur. Phys. J. D **13** (2001), 51.

[46] S. Keller and E. Engel, Chem. Phys. Lett. **299** (1999), 165.

[47] O. Kidun and J. Berakdar, *Many-particle spectroscopy of atoms, molecules, clusters and surfaces*, Kluwer Acad/Plenum Pub., New York, 2001.

[48] _____ , Surf. Sci. **507** (2002), 662.

[49] O. Kidun, N. Fominykh, and J. Berakdar, J. Phys. A **35** (2002), 9413.

[50] H. Knudsen and J. F. Reading, Phys. Rep. **212** (1992), 107.

[51] V. Kumar and Y. Kawazoe, Phys. Rev. B **63** (2001), 75410.

[52] D. L. Lichtenberger, *et al.*, Chem. Phys. Lett. **176** (1991), 203.

[53] R. W. Lof, M. A. Veenendaal, H. T. Jonkman, and G. A. Sawatzky, J. El.Spectr. Rel. Phenom. **72** (1995), 83.

[54] A. G. Lyalin, *et al.*, J. Phys. B **33** (2000), 3653.

[55] M. Madjet, C. Guet, and W. R. Johnson, Phys. Rev. A **51** (1995), 1327.

[56] F. Manghi, V. Bellini, and C. Arcangeli, Phys. Rev. B **56** (1997), 7149.

[57] J. L. Martins, *et al.*, Chem. Phys. Lett. **180** (1991), 457.

[58] S. Matt, *et al.*, J. Chem. Phys. **105** (1996), 1880.

[59] I. E. McCarthy and E. Weigold, *Electron-atom collisions*, Cambridge University Press, Cambridge, 1995.

[60] M. Mikami and I. Fukuda, Molecular Simulation **16** (1996), 375.

[61] T. Miura, *et al.*, Phys. Rev. A **62** (2000), 211201.

[62] J. P. Perdew and A. Zunger, Phys. Rev. B **237** (1981), 5048.

[63] S. Pollack, C. R. C. Wang, and M. M. Kappes, J. Chem. Phys. **94** (1991), 2496.

[64] M. E. Portnoi and I. Galbraith, Phys. Rev. B **60** (1999), 5570.

[65] E. Prodan and P. Nordlander, Chem. Phys. Lett. **349** (2001), 153.

[66] ——, Chem. Phys. Lett. **352** (2002), 140.

[67] A. Reinköster, U. Werner, N. M. Kabachnik, and H. O. Lutz, Phys. Rev. A **64** (2001), 23201.

[68] A. Rüdel, *et al.*, Phys. Rev. Lett. **89** (2002), 125503.

[69] P. Rudolf, M. S. Golden, and P. A. Brühwiller, J. Electr. Spectr. and Rel. Phenom. **100** (1999), 409.

[70] A. Russek, Phys. Rev. **132** (1963), 246.

[71] A. Russek and J. Bulman, Phys. Rev. **122** (1961), 506.

[72] A. Russek and J. Meli, Physika (Amsterdam) **46** (1970), 222.

[73] A. Russek and M. T. Thomas, Phys. Rev. **109** (1958), 2015.

[74] ——, Phys. Rev. **114** (1959), 1538.

[75] P. Scheier, *et al.*, Int. J. Mass Spectrosc. Ion Proc. **138** (1994), 77.

[76] M. Schmidt, *et al.*, Nature **393** (1998), 238.

[77] D. R. Schultz, R. E. Olson, and C. O. Reinold, J. Phys. B **24** (1991), 521.

[78] J. Seifert, K. Vietze, and R. Schmidt, J. Phys. B **29** (1996), 5183.

[79] K. Selby, *et al.*, Phys. Rev. B **43** (1991), 4565.

[80] H. Steger, *et al.*, Chem. Phys. Lett. **234** (1995), 455.

[81] V. Tarnovsky, *et al.*, J. Phys. B **31** (1998), 3403.

[82] M. Taut, Phys. Rev. A **48** (1993), 3561.

[83] M. Taut, A. Ernst, and H. Eschrig, J. Phys. B **31** (1998), 2689.

[84] J. P. Taylor, *Scattering theory*, John Wiley Inc., New York, 1972.

[85] E. Tossati and N. Manini, Chem. Phys. Lett. **223** (1994), 61.

[86] H. Tsuchida, A. Itoh, Y. Nakai, K. Miyabe, and N. Imanishi, J. Phys. B **31** (1998), 5383.

[87] D. A. Varshalovich, A. N. Moskalev, and V. K. Khersonskii, *Quantum theory of angular momentum*, World Scientific, Singapour, 1989.

[88] M. Vos, *et al.*, Phys. Rev. B **56** (1997), 1309.

[89] Y. B. Xu, M. Q. Tan, and U. Becker, Phys. Rev. Lett. **223** (1994), 61.

[90] C. Yannouleas and R. A. Broglia, Phys. Rev. A **44** (1991), 5793.

Eidesstattliche Erklärung.

Ich versichere hiermit, die vorliegende Dissertation:

Investigation of electronic correlations in nanostructures

selbständig verfasst und keine anderen als die von mir angegebenen Quellen und Hilfsmittel

verwendet zu haben. Den benutzten Werken wrtlich oder inhaltlich entnommene Stellen sind

als solche gekennzeichnet.

Halle, 11.11.2002 – O. Kidun –

Lebenslauf

Name: Oleg Kidun

geboren: 25.02.1969 in Maxatikha, Russland

Staatsangehrigkeit: Russland

Familienstand: verheiratet

Schulen und Ausbildung:

Sept. 1976 – Juni 1986   Grundschule und Gymnasium in Kashin bei Tver

Sept. 1986 – Juni 1989   Physikstudium an der Universitt Tver

Sept. 1989 – Juni 1999   Physikstudium an der Universitt Sankt-Petersburg

Sept. 1994 – Juni 1995   Anfertigung der Diplomarbeit
                          Thema: Thermodynamical extension of statistical ensembles
                          with Monte-Carlo simulations.
                          Betreuer: Prof. P. N. Vorontsov-Veliaminov

Sept. 1997 – Juni 1999   Anfertigung der Diplomarbeit zur Erlangung
                          des akademischen Grades Magister of Science.
                          Thema: Dynamical effect in the angular characteristics
                          of the core-level photoionization of oxygen
                          in the molecules CO and CO_2.
                          Betreuer: Prof. A. N. Pavlychev

seit Nov. 1999   Arbeit am Max-Planck-Institut fr Mikrostrukturphysik
                          zur Vorbereitung der Promotion
                          Betreuer: Prof. P. Bruno

Halle, 11.11.2002   – O. Kidun –

Elektronische Korrelationen in Nanostrukturen

Dissertation

von Oleg Kidun

Zusammenfassung

Zielen: Fortschritte bei der Entwicklung, Herstellung und Nutzung von Materialien, Instrumenten im Nanobereich hängen entscheidend davon ab, in wieweit man die Struktur und das Verhalten solcher Systeme auf der Ebene von Atomen, Molekülen und Clustern, kontrollieren und vorhersagen kann. Diese Doktorarbeit beschäftigt sich mit der theoretischen Behandlung der durch äußere Störungen induzierten charakteristischen Antwort von Nanosystemen, wie von Alkalimetall-Clustern, Fullerenen und Halbleiterquantenpunkten. Es wird gezeigt, daß das Verhalten solcher Systeme in externen Feldern durch ein Wechselspiel der Elektronenkorrelationen und der Finite-Size-Effekte bestimmt ist. Insbesondere wird der Einfluss der Polarisierbarkeit des Systems als Reaktion auf ein sich näherndes geladenes Teilchen, wie ein Elektron oder Proton, studiert. Zum Vergleich mit vorhandenen experimentellen Daten studieren wir den Ionisationskanal. Die Rolle von Austauscheffekten wird durch einen Vergleich der Ionisierungswahrscheinlichkeit des Systems durch Protonen oder Elektronen als Testladung aufgedeckt. Weiterhin untersuchen wir die Einzel- und multiple Photoionisation von Clustern.

Methoden: Sowohl approximative Methoden aus der Vielteilchentheorie als auch exakt lösbare Probleme werden für die Beschreibung der elektronischen Struktur des Systems herangezogen. Wir verwenden die Hartree-Fock-Theorie als Grundlage zu einer systematischen Behandlung der Elektron-Elektron-Wechselwirkungen. Dies geschieht störungs-theoretisch auf der Basis der random-phase approximation

für endliche Systeme. Die Anwendung der Hartree-Fock-Methode auf Systeme mit einer großen Anzahl von Elektronen erfordert die Berechnung einer immensen Zahl nichtlokaler Austauschintegrale und ist somit eine ernste technische Schwierigkeit. Somit ist das Finden einer Balance zwischen der Zuverlässigkeit der Ergebnisse und dem Rechenaufwand von entscheidender Bedeutung. Eine richtige Wahl des Rechenverfahrens ist deshalb der Schlüssel zur Behandlung von Systemen mit nichtlokalen Potentialen und mit einer großen Anzahl von Elektronen. Vor diesem Hintergrund wird in dieser Doktorarbeit ein neuer konzeptueller Zugang entwickelt, der es erlaubt, Systeme mit nichtlokalen Potentialen im Rahmen der variable phase approximation (VPA) zu behandeln. Zur numerischen wird weiterhin eine effiziente Finite-Differenz-Methode vorgeschlagen und angewendet. Es wird gezeigt, dass im Rahmen der vorgeschlagenen Methode nur der diagonale Bestandteil des nichtlokalen Ein-Elektron-Potentials zur Berechnung der Hartree-Fock-Integrale erforderlich ist. Basierend auf dem entwickelten VPA-Verfahren wird das Hartree-Fock-Problem für Systeme in Nanobereich neu formuliert und numerisch umgesetzt.

Hauptresultate: Die Ionisation von Vielelektronensystemen durch eine sich nähernde Testladung ist ein fundamentaler physikalischer Prozess, der direkte Einblicke in die Eigenschaften der korrelierten Elektronendynamik erlaubt. Die Ergebnisse der vorliegenden theoretischen Arbeit belegen, dass die Fluktuationen der elektronischen Ladungsdichte im Cluster den Ionisationswirkungsquerschnitt im niederenergetischen Regime unterdrücken. Diese Tendenz ist in völliger Übereinstimmung und erklärt zum ersten mal die experimentellen Daten für Fullerenen. Um das Wechselspiel zwischen dem Effekt endlicher Größe des Systems und nichtlokaler Abschirmeffekte zu beleuchten, werden Ionisationswirckungquerschnitte von Li-Clustern verschiedener Abmessungen und Elektronenzahl miteinander verglichen. Es stellte sich heraus, daß mit zunehmender Größe - und demzufolge auch mit einer anwachsenden Zahl von delokalisierten Elektronen - die Teilchen-Loch-Anregungen eine wichtige

Rolle in der Bestimmung der Ionisationswirkungsquerschnitte der Cluster spielten. Tatsächlich beobachten wir, daß der Einschluß dynamischer Abschirmung zu einer Glättung des Ionisationswirkungsquerschnitts bei zunehmender Cluster-Größe führt, während die Vernachlässigung dieses Phänomens eine gegenteilige Tendenz zeigt.

Die Rolle der Austauschwechselwirkung wird durch den Vergleich der Proton- und Elektronstoßionisation von C_{60} untersucht. Die Abwesenheit der Austauschwecheselwirkung zwischen dem Proton und den Targetelektronen führt dazu, dass ein Teil der Teilchen-Loch-Anregungen ausfallen. Als Folge stellen wir fest, dass Protonen Metallcluster und Fullerene effektiver als Elektronen ionisieren.

Für die Beschreibung der mehrfachen Ionisation von Fullerenen durch ein einzelnes Photon wird zum ersten Mal das statistische Energiedepositionsmodell herangezogen. Dazu werden die o.g. ab-initio-Berechnungen der einfachen Ionisation verwendet. Die Theorie erlaubt einen relativ einfachen Zugang zu den materiellen, strukturellen und energetischen Abhängigkeiten der mehrfachen Ionisationsprozesse. In dieser Arbeit werden erstmals die Wahrscheinlichkeiten von verschiedenen mehrfachen Photoionisationsreaktionen in C_{60} berechnet.

Eines der wenigen genau lösbaren quantenmechanischen Probleme ist das Problem von zwei wechselwirkenden Elektronen im parabolischen Potential. Unter Verwendung der Zweielektronen-Wellenfunktion wird der Doppelphotoionisationsquerschnitt eines Quantenpunkts berechnet und die Winkel- und Energieverteilungen untersucht. Es wird gezeigt, dass die Doppelphotoionisationsspektren direkte Informationen über die korrelierte Zweielektronen-Dichte enthalten und dazu geeignet sind, Korrelationen in Quantenpunkten abzubilden.

Zukünftige Anwendungen: Die Resultate dieser Arbeit sind auf Probleme anwendbar, die sich mit beliebigen nichtlokalen oder impuls-abhängigen Potentialen befassen und auf beliebige Systeme von Integro-Differentialgleichungen. Desweiteren sind sie eine theoretische Basis für die experimentellen Untersuchungen des Einflusses von Finite-Size-Effekten auf die Stärke der elektronischen Korrelationen. Die meisten unserer Resultate können mit Hilfe moderner Koinzidenzspektroskopiemethoden direkt experimentell überprüft werden.

Summary

Advances in the development, fabrication and utilization of nano-scale materials, devices and systems are driven by the ability to control their structure and response on the nano-meter scale, that is at the level of atoms, molecules and clusters. This thesis deals with the theoretical treatment of the characteristic response to external perturbations of nanosystems, such as alkali-metal clusters, fullerenes and semiconductor quantum dots. It is shown that this response is determined by an interplay between electronic correlations and finite-size effects. Particular attention is devoted to the following many-body phenomena and collision processes: The polarization of the system in response to an approaching charged particle, such as electrons or protons. For a comparison with available experiments we considered the ionization channel. The role of exchange effects is revealed upon a comparison of ionization probability of the target by protons and electrons. We also investigate the single and the multiple photoionization of clusters.

Both approximate many-body methods and exactly solvable problems are employed for the description of the electronic structure of the systems. We use the Hartree-Fock (HF) theory as a basis and account systematically for the electron-electron interactions in a perturbative way using the random phase approximation with exchange.

The Hartree-Fock method, while formally well-established, represents severe technical difficulties in the application to the systems with a large number of electrons due to the presence of a huge number of the nonlocal exchange integrals. This essentially complicates the calculations, so that the finding a balance between the reliability of the results and the computational costs becomes an important, if not a decisive, issue. Therefore the right choice of the calculational procedure is the key question for solving nonlocal potential problems for systems with large number of electrons. To increase

the efficiency of Hartree-Fock calculations, we develop in this thesis a new conceptual framework, based on the extension of the variable phase approach (VPA) to nonlocal potentials. In the VPA the solution of quantum-mechanical problems is formulated in terms of observables, e.g. scattering phase shifts and scattering amplitudes, rather than by means of the wave functions. We also propose the efficient finite-difference scheme for a numerical implementation. The advantage of this scheme stems from the fact that for the calculation of the Hartree-Fock integrals only the diagonal part of the nonlocal one-electron potential is required. Based on the developed VPA scheme, we reformulate the Hartree-Fock problem for nano-size systems.

The ionization of many-electron systems by a charged particle is a fundamental physical process, allowing a direct information on the correlated electron dynamics. The fluctuations of the electronic charge density of the clusters, accounted for within the random phase approximation with exchange, are shown to suppress the single ionization channel in the low-energy region, while at large impact energies they are not essential. This tendency is in full agreement with the experimental data for fullerene clusters. In contrast, the calculations performed without the account of the dynamic screening were unable to reproduce the experimental data, giving a wrong low-energy behavior of the ionization cross section. Our first principle numerical results are interpreted with the help of the Thomas-Fermi model of screening. The qualitative conclusion of this study is that the change of the effective radius of the inter-electron interaction does not lead to a simple scaling of the ionization probability, as it could be supposed, but modifies also its energy dependence. In addition, we investigate the interplay between quantum size and nonlocal screening effects by tracing the changes in the ionization cross sections for Li clusters with an increasing cluster radius. The particle-hole excitations proved to play a decisive role in the evolution of the ionization cross sections of the clusters with the increase of their size and, consequently, with the increase of the number of delocalized electrons. Actually,

we observe that the inclusion of the dynamic screening leads to the flattening of the ionization cross section as the cluster size grows, while the disregard of this phenomenon gives the opposite tendency. What is less obvious, the energy position of the maximum in the cross section also shifts in the opposite directions. It is hoped that these striking size effects will stimulate further experimental measurements. A specific sort of correlation effects arising from the exchange interaction is traced down via a comparison of the proton and the electron impact ionization of C_{60}. The absence of the exchange between the proton and the target electrons qualitatively plays the same role as the disregard of the particle-hole (de)excitations in the many-electron system. In particular, the $\sim 30\%$ increase of the proton impact ionization probability as compared to the electron impact is observed.

For the description of the multiple ionization of fullerenes by a single photon, the statistical energy deposition model is used for the first time. Usually, the calculations based on this model employed adjustable or semi-empirical parameters for the estimation of the single ionization transition amplitude, which enters the expression for the multiple ionization probability. We improve this step by performing the first principle calculations of this quantity. In doing this we get a natural access to the material, structural and energy dependence of the multiple ionization processes. For the first time the probabilities of different multiple photoionization reactions in C_{60} are estimated and compared. The diffraction of the photoelectron wave on the fullerene shell is shown to be a prominent feature of these processes.

One of the few exactly solvable quantum-mechanical problems is the problem of two electrons, coupled via bare Coulomb repulsion, in the parabolic confinement. Using the exact two-electron wave function, the double photoionization cross section of a quantum dot is derived and the various angular and energy spectra are calculated. The mapping of the two-electron density onto the double photoionization spectra is suggested as a promising tool for the visualization of subtle correlation effects.

The results of this work are applicable to problems dealing with arbitrary non-local or momentum-dependent potentials, to arbitrary systems of integro-differential equations and as a theoretical background for the experimental investigations of the influence of finite size effects on the strength of the electronic correlation. Most of our results can be directly verified experimentally using modern many-particle coincidence spectroscopic techniques.